

RFNC-VNIIEF
Los-Alamos National Laboratory

LA-SUB--95-194

**RESULTS OF ALUMINIUM COMPOSITE BEHAVIOUR
RESEARCH UNDER DYNAMIC LOADS**

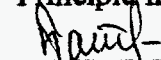
(2 stage of contract 0002 P 0004-95 task 3)

Contract manager,

RFAoS, professor

 S.A. Novikov

Principle investigator, DPL

 Yu.V. Bat'kov

DISTRIBUTION OF THIS DOCUMENT IS UNLIMITED



MASTER

Arzamas-16, 1995

DISCLAIMER

This report was prepared as an account of work sponsored by an agency of the United States Government. Neither the United States Government nor any agency thereof, nor any of their employees, make any warranty, express or implied, or assumes any legal liability or responsibility for the accuracy, completeness, or usefulness of any information, apparatus, product, or process disclosed, or represents that its use would not infringe privately owned rights. Reference herein to any specific commercial product, process, or service by trade name, trademark, manufacturer, or otherwise does not necessarily constitute or imply its endorsement, recommendation, or favoring by the United States Government or any agency thereof. The views and opinions of authors expressed herein do not necessarily state or reflect those of the United States Government or any agency thereof.

DISCLAIMER

Portions of this document may be illegible in electronic image products. Images are produced from the best available original document.

ABSTRACT

Report is prepared in accordance with stage 3.3 of subcontract 0002 P 0004-95, task 003, between Russia Federal Nuclear Center - All-Russia NII of Experimental Physics (RFNC-VNIIEF) and Los-Alamos National Laboratory (LANL) "Study of Aluminium Composite Plastic Deformation Resistance and Destruction under Dynamic Loads".

The report presents the results of physical and mechanical property study for aluminium composite A 359 DURAL from San-Diego under dynamic and shock-wave loads.

The report was prepared by a team of VNIIEF specialists: S.A.Novikov, Yu.V.Bat'kov, V.A.Pushkov, A.B.Glushak, V.A.Ogorodnikov, M.V.Zhernokletov, V.I.Skokov, N.D.Fishman, A.N.Lebedev.

English translation was done by Panevkina E.I.

CONTENTS

INTRODUCTION.....	4
1. MATERIALS.....	5
1.1 Samples.....	5
1.2 Macro- and microstructure, microhardness.....	5
2. ELASTIC PROPERTIES.....	6
3. STRESS-STRAIN DIAGRAMS.....	7
3.1 Tension diagrams.....	7
3.2 Compression diagrams.....	8
4. CRACK RESISTANCE.....	9
5. DYNAMIC COMPRESSIBILITY.....	11
6. DYNAMIC ULTIMATE YIELD.....	12
7. SHEAR STRENGTH.....	13
8. SPALL STRENGTH.....	16
8.1 Plate impact.....	16
8.2 Explosive loading.....	19
8.3 Temperature effect.....	20
8.4 Metallographic study.....	20
CONCLUSIONS.....	22
REFERENCES.....	23

INTRODUCTION

According to task 003 of subcontract 0002 P 0004-95 between RFNC-VNIIEF (Russia) and LANL (USA). "Investigation of destruction and resistance to plastic deformation of composite materials under dynamic loads". VNIIEF does the research of aluminium composite (AL+20%SiC) behaviour which is delivered by LANL, under dynamic and quasistatic loads.

At stage 3.2 (task 1), report [1] was prepared which gives the description of the techniques, facilities and devices used by VNIIEF to study the material behaviour. For each technique the results of typical composite material research were presented which illustrate its capabilities. Three blanks of aluminium composite A359 DURAL from San-Diego were obtained in February 1995 which total weight was 63kg; and according to the prepared drawings the samples were fabricated for tests.

This report prepared according to task 3.3 (stage 2) of the contract contains the research results of physical and mechanical properties of the aluminium composite under dynamic and shock-wave loads.

1. MATERIALS

1.1 SAMPLES

The efforts were aimed at the study of LANL delivered aluminium composite - alloy A 359 of DURAL company from San-Diego which is aluminium alloy A 356 modified with high Si content. Stichiometric composition of aluminium composite (AC): base-Al; 8.5-9.5% Si; 0.02% Fe; 0.02% Cu; 0.1% Mn; 0.45-0.6% Mg; 0.02% Ti; 0.2% Sn.

The research samples of 10 types were fabricated in VNIIEF according to specially developed drawings A0311-L233.000 out of three blanks \varnothing 180mm and 360mm, 320mm, 360mm long. Figure 1 shows the geometry of blank cutting for sample fabrication (along and across the blank axis). Figure 2 presents the pictures of the samples to study the AC dynamic properties.

After the samples were fabricated of LANL blanks, they were heated to 530° C for 8 hours and cooled down in the hot water and subsequently cooled in the air (regime T-6). The measured sample density was $\rho_0 = 2.760 + 2.779 \text{g/cm}^3$.

1.2 MACRO- AND MICROSTRUCTURE, MICROHARDNESS

The delivered aluminium composite (AC) was metallographically studied with witness-samples cut out of one blank as received and after thermal treatment. Figure 3 presents the cutting geometry for the witness-samples for the studies (the sample surfaces for microsections to be made are cross-hatched). The metallographic study included the analysis of macro- and microstructures and identification of material microhardness in the witness-samples on the surfaces marked in fig.3 and by the technique presented in ref.[1]. The aluminium composite as received and after thermal treatment has the structure of the aluminium base comprising dendrites of the solid solution of aluminium and silicon (of maximum 1.65% silicon contents according to Al-Si state diagram) and aluminium-silicon eutectics (of 12.7% silicon contents according to Al-Si state diagram) with sprinkled SiC particles (fig.4a). The material is characterized by macro- and microheterogeneity, namely, uneven SiC particle distribution in the aluminium base (fig.4b). Almost in all studied witness-samples as received (11 samples) and after thermal treatment (11 samples) large zones are seen which completely lack the carbide constituent (in figs. 5a, b-dark areas, in figs. 5c and 4b-light areas). SiC particles are 0.014mm large in average, however big particles of 0.16mm are also observed (fig.4c).

The microhardness of the aluminium base as received is 103.6kg/mm^2 , in average, and after thermal treatment - 123.2kg/mm^2 , i.e. its slight increase is observed as a result of thermal treatment, by 19.6kg/mm^2 approximately. The difference between the microhardness of the solid aluminium solution with silicon is negligible. The microhardness of silicon carbide particles as received is 3023kg/mm^2 , in average, and after thermal treatment - 3426kg/mm^2 , i.e. its increase is also observed as a result of thermal treatment by 403kg/mm^2 in average.

2. ELASTIC PROPERTIES

Pulsed ultrasonic method similar to the described in ref.[2] was used to measure the velocities of elastic wave and elastic modulus propagation for the aluminium composite.

According to this method, thin piezoelectrical converters were connected to the ends of a cylindrical sample: an emitter and a receiver of short ultrasonic pulses. The time intervals were measured from the beginning of emission till different ultrasonic wave pulse arrival at the receiver. Based on the measured times, the velocities of longitudinal and transversal elastic wave propagation in the sample material were calculated. Elastic moduli were calculated based on the obtained velocities and sample densities.

To do the measurements, 3 cylindrical samples 10mm in diameter and 25mm high were prepared and cut along the blank axis. Table 1 shows the resultant measured velocities of elastic waves C_l (longitudinal), C_t (transversal) and calculated elastic moduli at confidential probability $P=0.95$.

Table 1.

Elastic Wave Velocities and Elastic Moduli
for Aluminium Composites

Name	Value	Confidential interval, \pm
Density ρ_0 , g/cm ³	2.761	0.001
Longitudinal wave velocity C_l , km/s	7.16	0.04
Transversal wave velocity C_t , km/s	3.767	0.015
Plane wave modulus, ρC_l^2 , GPa	141.5	1.7
Shear modulus G , GPa	39.2	0.3
Bulk compression modulus K , GPa	89.2	1.3
Young's modulus E , GPa	102.6	0.9
Poisson's coefficient ν	0.3083	0.0012
Acoustic resistance ρC_l	19.77	0.12
Sound velocity C_0 , km/s	5.68	0.04

3. STRESS-STRAIN DIAGRAMS

With the techniques described in ref.[1] the dynamic mechanical properties of the aluminium composite were studied:

- tension diagrams at $T=25^{\circ}\text{C}$ and strain rates $\dot{\epsilon}=200-260\text{ s}^{-1}$ (4 tests);
- compression diagrams at $T=-50, 25, 100, 300^{\circ}\text{C}$ and strain rates $\dot{\epsilon}=200-500\text{ s}^{-1}$ (13 tests).

3.1 TENSION DIAGRAMS

The samples of reverse type in the form of a thimble [1] were tested which had a working length of 8mm, four through grooves and 40mm^2 working cross-section. The samples were cut out of a cylindrical blank perpendicular to its axis (direction 1) and parallel to its axis (direction 2).

Figure 6a gives a typical tension diagrams $\delta-\epsilon$ for the aluminium composite at 25°C and 200s^{-1} strain rate. Here, also in fig. 1b the strain relationship $\epsilon=\epsilon(t)$ in this test is shown which was used to determine strain rate $\dot{\epsilon}$. As it is seen from fig. 6b, during the first $\sim 15\text{ms}$ the strain rate grows from zero to its value $\dot{\epsilon}=\text{const} = 200\text{s}^{-1}$. The similar picture was seen in other tests.

As the tests have shown, the aluminium composite at 25°C resists slightly to the dynamic tension and destructs frangibly via normal detachment. Provided, in all tests the destruction took place at $\sim 0.2\%$ deformations. Fragile destruction of the samples resulted in the fact that yield strengths $\sigma_{0.1}$ and $\sigma_{0.2}$ were almost equal and corresponded to ultimate strength σ_{km} in each individual test.

Table 2 presents the test results at 25°C .

Table 2.

N test	T, $^{\circ}\text{C}$	$\dot{\epsilon}$, s^{-1}	$\sigma_{0.2}$, MPa	σ_{km} , MPa	Cut direction
1	25	200	260	260	1
2		260	240	240	1
3		240	220	220	1
4		250	280	280	2

3.2 COMPRESSION DIAGRAMS

The samples in the cylindrical geometry 8mm in diameter, 8mm long, 50mm² working section were tested. The samples were cut out of the blank both in direction 1 and direction 2 (see subsection 3.1).

Figure 7 gives a typical compression diagram σ - ϵ for the aluminium at 25°C and strain rate 390s⁻¹. Here also, in fig.7b strain relationship $\epsilon=\epsilon(t)$ is shown for this test, which demonstrates that the test strain rate was constant ($\dot{\epsilon}=\text{const}$) as a whole. Diagram σ - ϵ shows that in the plastic section of the diagram a considerable strain hardening appears.

Table 3 presents the results of all tests at T=-50-+300°C. Here, except the temperature, the test numbers are shown as well as strain rate $\dot{\epsilon}$, ultimate strength $\sigma_{0.2}$ and the direction of sample cut out of the blank (see subsection 3.1).

Table 3.

N test	T, °C	$\dot{\epsilon}$, s ⁻¹	$\sigma_{0.2}$, MPa	Cut direction
1	-50	320	370	2
2		460	380	2
3		300	450	2
4	25	390	425	1
5		320	375	1
6		340	370	1
7		310	385	2
8	100	340	330	1
9		380	290	1
10		390	340	2
11	300	370	260	2
12		200	270	2
13		500	330	2

4. CRACK RESISTANCE

Crack resistance study was done with technique [1] at $T = -50, 25, 100, 300^{\circ}\text{C}$ and relative load rates $\bar{V} = (0.63-1.40) \cdot 10^4 \text{ s}^{-1}$ (13 tests).

Plane samples were tested with a wedgeshape cut, 24mm wide, 20mm high, 14mm thick and of 196mm^2 nominal cross-section. The samples were cut both in direction 1 and direction 2 (see subsection 3.1).

Figure 8 presents typical P- Δ diagram for the aluminium composite at 25°C and relative load rate $\bar{V} = 1.40 \cdot 10^4 \text{ s}^{-1}$. Magnitudes of dynamic crack resistance K_{1d} were derived from the value of critical force P_c . The magnitude of P_c was taken from P- Δ diagram in the point of diagram crossing with a straight line which slope tangent is by 5% smaller than the slope tangent of the initial section of the diagram. Providing, in the resultant P- Δ diagrams relation $P_{\text{max}}/P_c < 1.1$ was met (P_{max} - maximal load in the diagram) that is one of the conditions of test correctness [2].

We could not manage to develop initial cracks in the samples because the aluminium composite is of considerable brittleness. In the attempts to create an initial crack the sample was either broken in two halves or a rather long crack was formed that did not allow to conduct the tests correctly and to define K_{1d} magnitude. So, the tests were accomplished with the samples of no initial cracks. Prior to the tests a colibration function Y was determined for the polymetyl methacrylate (PMMA) samples with known K_{1d} , including the samples without initial cracks. The samples of PMMA were identical in size to the samples of aluminium composite and for their tests the same scheme of force applications was employed. So, calibration function Y obtained for PMMA samples could be used also for the aluminium composite samples.

Table 4 given the results of all tests at $T = -50$ to $+300^{\circ}\text{C}$. Here, except the temperature the test members are shown as well as the values of relative load rate \bar{V} , dynamic crack resistance K_{1d} and the direction of sample cut of the blank (see subsection 3.1).

Table 4.

N test	T, $^{\circ}\text{C}$	\bar{V} , s^{-1} .	K_{1d} , $\text{MPa} \cdot \text{m}^{1/2}$	Cut direction
1	-50	$0.98 \cdot 10^4$	10.0	2
2		$1.04 \cdot 10^4$	9.8	2
3		$0.91 \cdot 10^4$	10.5	2

4	25	$1.20 \cdot 10^4$	10.4	1
5		$1.40 \cdot 10^4$	10.8	1
6		$1.14 \cdot 10^4$	9.8	2
7		$1.00 \cdot 10^4$	10.5	2
8	100	$1.10 \cdot 10^4$	16.2	2
9		$1.20 \cdot 10^4$	16.5	2
10		$1.30 \cdot 10^4$	17.4	2
11	300	$0.63 \cdot 10^4$	38.4	2
12		$0.70 \cdot 10^4$	40.5	2
13		$0.64 \cdot 10^4$	41.2	2

Let us note that the first batch of test samples was cut of the blank in direction 1. Partially these samples were spent in the attempts to get initial cracks and to develop the loading modes. Later, the samples cut in direction 2 were delivered for tests. So, with the limited number of the first samples the crack resistance tests of the composite cut in various directions were conducted only at 25° C. The tests at T=50, 100, 300° C were done with the samples cut out of the blank only in direction 2.

The tests showed that the aluminium composite is of low crack resistance and at the noted temperatures it is destructed frangily. Thus, at 25° C and $\bar{V} = (1.0-1.4) \cdot 10^4 \text{ s}^{-1}$ average value K_{Ia} constitutes $\sim 10.4 \text{ MPa} \cdot \text{m}^{1/2}$.

5. DYNAMIC COMPRESSIBILITY

To obtain the data on dynamic compressibility we used an impedance matching method [4]. According to this method the studied samples were placed in the way of shock wave propagation behind the metal shields of known shock adiabats. Shock wave strength was varied with explosive throwing systems accelerating metal impactors to different velocities. In the experiments, shock wave velocities U_s were measured in the studied samples. Other characteristics: shock compression pressure P , mass velocity of the substance motion behind the wave front U_p , specific density ρ and volume V - were calculated based on U_s values and shock wave parameters known from special experiments in the shields, assuming the pressures and mass velocities are equal at the shield - sample interface and accounting the laws of mass and momentum conservation. The expansion isentropes of the copper and aluminium shields in P - U_p coordinates were identified with the mirror reflections of shock adiabats. Copper and aluminium shock adiabats were taken in the form of linear U_s - U_p relations [5]:

$$U_s = 3.915 + 1.495 U_p \quad (\text{for Cu})$$

$$U_s = 5.33 + 1.356 U_p \quad (\text{for Al})$$

Electrocontact and piezoceramic gages placed at different sample levels were used to record the shock wave velocities in the samples [6]. The samples of $\rho_0 = 2.78 \text{g/cm}^3$ density were fabricated in the form of pellets 12mm in diameter and 3-4mm high.

The experiment results are shown in table 5 which also presents the shield materials and mass velocities U_p in them. The table values of wave velocities U_s correspond to the average result of 4-5 independent experiments.

Graphically the obtained data are shown in U_s - U_p diagram (fig.9) where they are described by the linear relation:

$$U_s = 5.54 + 1.356 U_p, \text{ km/s}$$

Table 5.

	Loading device		Shock wave parameters in sample			
	U_p , km/s	U_s , km/s	U_p , km/s	P , GPa	ρ , g/cm ³	V , cm ³ /g
Cu	0.25	6.03	0.35	5.87	2.95	0.339
Cu	0.52	6.60	0.71	13.03	3.115	0.321
Al	0.91	6.73	0.89	16.65	3.204	0.321
Al	1.13	6.94	1.12	21.61	3.315	0.302
Al	1.465	7.49	1.43	29.78	3.436	0.291
Al	1.70	7.70	1.67	35.75	3.55	0.282
Al	2.09	8.44	2.04	47.86	3.666	0.273
Al	2.70	9.12	2.65	67.19	3.919	0.255

6. DYNAMIC ULTIMATE YIELD

To obtain the information on dynamic strain at strain rate $\dot{\epsilon} = 10^3 - 10^4$ 1/s, a direct Taylor method was used [7]. The experimental set for Taylor method [1] includes an acceleration unit for cylindrical samples and measurement equipment. The diameter of a runaway barrel is 20mm at 1200mm length. A barrier-30XGSA steel plate hardened to RH=40 - was placed at ~ 200 mm from the barrel cut. Electromagnetic gages were used to measure the velocity of a shell-sample in each test at the barrel output. The velocity measurement error - $\pm 5\%$. Figure 10 gives general views of composite samples before and after the impact. Initial diameter of the shell-sample - 20mm, initial length - 100mm. Table 6 gives the collision velocities W_0 , finite length L_k ; dynamic ultimate yield σ_T' derived classical Taylor formula $\sigma_T' = -\rho_0 W_0^2 / 21 \ln(L_k/L_0)$ as well as σ_T'' value derived from mathematically treated data.

Table 6.

W_0 , m/s	L_k , mm	σ_T' , GPa	σ_T'' , GPa
110	97	0.55	0.4
155	94	0.54	
170	93	0.55	

In fig. 10 it is evident that in the sample tested at $W_0 = 170$ m/s the cracks came up. At higher velocities the sample was destructed.

Numerical modeling of a strained sample at its deceleration was done in the elastic - plastic approximation. The system of equations was formulated in Lagrange variables. Ball constituents of stress and strain gages were coupled via Mi-Gruneizer equation of state. For each test result will a research approximation, constant value σ_T was found at which a calculated finite length of shell-sample L_k and its shape coincide well with their test values. Finally, it was found that the test results are well described by constant $\sigma_T = 0.4$ GPa. Figure 11 shown the calculation results. The calculations done with classic Taylor formula give higher values than the numerical modeling results for value σ_T .

7. SHEAR STRENGTH

The resistance of aluminium composite to plastic deformation or shear strength along side with compressibility, viscosity and elasticity, is one of the basic reological properties of a solid body which are needed to describe its behaviour under high-rate strain, including shock waves (SW).

The shear strength characterized by dynamic ultimate yield Y_g under SW compression was studied by measurements of main stresses σ_x (longitudinal) and σ_y (transversal) which are described in detail in ref. [1]. From the viewpoint of elastic-plastic model $Y_g = \sigma_x - \sigma_y = 2\tau$ at $\sigma_x > \sigma_{HE}$, where σ_{HE} - amplitude of Hugonio elastic limit, τ - shear stress.

By the established considerations with a 1-D deformation of elastic-plastic body in the plane shock wave:

$$\begin{aligned} \sigma_x &= \sigma_0 + 2/3 Y_g; & \sigma_y &= \sigma_0 - 1/3 Y_g; \\ \sigma_0 &= (\sigma_x + 2\sigma_y)/3; & Y_g &= (1-\nu/1-2\nu)\sigma_{HE} \quad \text{at } \sigma_x = \sigma_{HE} \end{aligned}$$

where σ_0 - a ball constituent of the stress dyadic.

In the range of shock compression stresses from 2.3GPa to 22GPa, 15 tests were accomplished with 9 types of explosive contact devices of known SW parameters in the shields. Figures 12.14 present several oscillograms of recorded main stress profiles σ_x and σ_y in the aluminium composite samples.

The experiment results are summed up in table 7 where in order the following is presented: studied material, explosive loading device shield material, mass velocity U_s in the shield, measured velocities σ_x , σ_y , calculated average stress σ_0 , dynamic ultimate yield $Y_g = \sigma_x - \sigma_y$ and ratio σ_0/σ_x characterizing non-hydrostaticity of the stressed state of the aluminium composite behind plane SW front.

The study results have shown that the dynamic ultimate yield Y_g as the main stress difference, characterizing the shear strength of a shock compressed material and determining the shock adiabat deviation from the quasi hydrostatic compression, is almost constant and equals $Y_g = 0.24\text{GPa}$ for the aluminium composite in the studied range of shock compression stresses σ_x from 2.3GPa to 22GPa. High anisotropy of the stressed state behind SW front in the aluminium composite in the range of low stresses ($\sigma_0/\sigma_x = 0.9$ at $\sigma_x = 2.35\text{GPa}$) decreases rather quickly with σ_x growth (even at $\sigma_x = 11.5\text{GPa}$ $\sigma_0/\sigma_x = 0.99$).

The measured test values for longitudinal stress σ_x within the measurement error ($\pm 8\%$) coincide with σ_x values calculated in the solution of the problem on arbitrary rupture decay with the account of the obtained shock adiabat (see

section 5) and the known parameters of shock waves in the shields. Values of U_s and U_p obtained with manganine gauges are given also in table 7 and fig. 9.

Table 7.

Resultant measured main stress in
aluminium composite

№	Loading device		Stresses, GPa				σ_0 / σ_x	U_s , km/s	U_D , km/s	Notes
	Shield material	U_0 , km/s	$\sigma_x \pm 8\%$	$\sigma_y \pm 8\%$	σ_0	$Y_g = 2\tau$				
1	Copper M1	0,098	2,3	2,0	2,10	0,3	0,91	6,28	0,135	
2			2,4	2,0	2,13	0,4	0,89			
3	Copper M1	0,175	3,6	3,4	3,47	0,2	0,96	5,65	0,23	
4			3,6	3,3	3,40	0,3	0,94			
5	Copper M1	0,18	3,9	3,7	3,77	0,2	0,96	5,75	0,24	
6			3,8	3,6	3,67	0,2	0,96			
7	Copper M1	0,22	5,1	4,8	4,90	0,3	0,96	5,92	0,305	
8			4,9	4,7	4,77	0,2	0,97			
9	Copper M1	0,35	8,5	8,3	8,37	0,2	0,98	6,39	0,48	
10		0,35	8,6	-	-	-	-			
11	Copper M1	0,47	11,5	11,3	11,37	0,2	0,99	6,43	0,645	
12		0,52	13,0	12,8	12,87	0,2	0,99	6,66	0,705	
13	Aluminium AD1	0,91	16,9	~16,6	16,70	~0,3	0,99	6,89	0,895	
14										
15	Aluminium AD1	1,15	21,8	~21,6	21,66	~0,2	0,99	6,90	1,140	
16										

8. SPALL STRENGTH

8.1 PLATE IMPACT

To do the study of the spallation strength by continuous recording of sample free surface motion with a capacitive velocity gage, facility BUT-76 [9] was used which is based on a ballistic shock tube for projectile runaway with a measuring set (fig.15). The recorded "history" of current velocity of the free surface holds the information on the spallation kinetics. The studied sample (4) 50mm in diameter and 5-10mm thick was placed in the aluminium cartridge which was mounted at the 76.2mm caliber and 10.8mm long barrel headpiece end. Shell (5) of 0.2-0.8kg mass with an impactor of aluminium or aluminium composite 2.5-5mm thick is accelerated in the evacuated barrel by the compressed air energy. With the plane collision of the impactor (3) with the sample (4), slant angle does not exceed $0.5 \cdot 10^{-3}$ rad at 50mm diameter. The barrel headpiece (1) is coupled with the braking chamber (2) which facilitates soft deceleration of the loaded sample and preserves it for the further metallographic analysis. The facility is equipped with the measuring set which measures the flying up velocity W of the impactor and free surface velocity profile $W(t)$ of the studied sample. The velocity profile was measured with a capacitive gage at $\pm 10\%$ accuracy. The impactor flying-up velocity is measured with electrocontacts at higher accuracy $\pm 0.5\%$ that allows to accomplish reliable norming of $W(t)$ function. The sizes of impactor (Δ_{α}) - target (Δ_m) pairs were chosen to provide for uniform strain and constituted 2.5-5.0 and 5.0-10.0mm. For each noted impactor - target pair 5-6 tests were conducted in which impactor velocity was measured to implement the following loading conditions for the samples in the target which are controlled with metallographic analysis (see subsection 8.4). A - no destruction nuclei observed in 200 time magnified microsections of sample longitudinal sections; B - separate nuclei of destruction in the form of micropores appeared in the spallation plane; C - coalescence of separate destruction nuclei in a main crack; D - complete sample destruction in pieces. In each test with the capacitive gage with the protective ring the continuous recording of sample face surface velocity $W(t)$ was done (Figs. 16,17). The information obtained in the tests was used to define several characteristics of the sample material with the following relationships:

$$\sigma_p = 0.5 \rho_0 C_0 (\Delta W + \delta W);$$

$$\sigma_0 = 0.5 \rho_0 C_0 W_0; \quad \sigma_{HE} = 0.5 \rho_0 C_1 W_d;$$

$$\dot{\epsilon} = 1/2 (\partial W / \partial t) (1/C_0);$$

$$\delta W = 1/2 \frac{\partial W}{\partial \alpha} \left(\frac{\delta}{C_0} - \frac{\delta}{C_1} \right);$$

$$\lambda = (\sigma_0^2 + \delta) / E \frac{(1 + \nu)(1 - 2\nu)}{(1 - \nu)}$$

where $\rho_0 = 2.77 \text{g/cm}^3$; $C_0 = 5.68 \text{km/s}$; $C_1 = 7.16 \text{km/s}$; $E = 102.6 \text{GPa}$; $\nu = 0.308$ - material constants; $\Delta W = W_2 - W_1$ - difference in the velocities in the first maximum - W_1 and first minimum of $W(t)$ function, $\partial W / \partial t$ - $W(t)$ graph slope in front of W_2 ; W_a - elastic precursor amplitude; σ_0 , σ_p , σ_{HE} - pressure in the shock wave, tensile stress and Hugonio ultimate yield; $\dot{\epsilon}$ - strain rate of the material in the spallation area; λ - specific material tearing per surface area unit (destruction energy); δ - tearing thickness; T - duration of compression wave oscillation in the spallation layer. Table 8 presents this information quantitatively.

The analysis of obtained results testifies for the fact that under the rectangular stress pulse of ~ 0.7 - 1.5ms and $\sigma_0 = 1$ - 2GPa the samples are destructed at $\sigma_p = 0.52$ - 0.65GPa and $\dot{\epsilon} = (8.8 \cdot 10^3 - 1.4 \cdot 10^4) \text{s}^{-1}$ or $\lambda = 3$ - 6J/cm^2 . The sample destruction is nucleated in the form of micropores and microcracks both in aluminium and in incorporated filler that explains a somewhat lower strength of ceramic material compared to the metal aluminium. Providing the destruction of large-scale samples occur at although lower impactor velocities but at higher stored elastic energy in it. The width of material destruction zone in the larger samples ($\Delta = 10 \text{mm}$) constitutes $\sim 1.1 \text{mm}$ and in smaller samples ($\Delta = 5 \text{mm}$) $\sim 0.4 \text{mm}$. That is, under the studied sample destruction an evident scale effect of the energy nature manifests itself.

In all tests a two-wave configuration of the shock wave was observed (see figs. 16,17). Elastic precursor amplitude is $\bar{W}_a = 17 \text{m/s}$ that corresponds to Hugonio ultimate yield $\sigma_{HE} = 0.17 \text{GPa}$

Table 8

**Results of Spall Strength Study
at Plate Impact**

Δx , Δm mm- mm	W_0 m/s	W_1 m/s	W_2 m/s	W_{cl} m/s	$(\partial W/\partial t)10^{-6}$ m/s ²	σ_{HE} GPa	σ_0 GPa	σ_D GPa	λ J/sm ²	$\dot{\epsilon}$ s ⁻¹	T ms	C_1 km/s	Degree of damage
5-10	123.1	104.5	-	10	-	0.10	0.97	-	3.3	-	-	-	A
	166.9	130.8	54.9	10	105	0.10	1.32	0.60	6.1	$9.2 \cdot 10^3$	1.65	7.2	C
	172.9	148.0	77	17	100	0.17	1.36	0.65	6.4	$8.8 \cdot 10^3$	1.70	77.1	C
	207.0	200	130	17	105	0.17	1.63	0.64	9.2	$9.2 \cdot 10^3$	1.70	7.1	D
2.5-5	156.7	129.9	-	10	-	0.10	1.24	-	2.7	-	1.50	6.7	A
	163.2	133.5	-	21	-	0.21	1.29	-	2.9	-	1.45	6.9	A
	173.9	153	94.3	16	160	0.16	1.37	0.53	3.3	$1.4 \cdot 10^4$	0.86	7.0	B
	193.2	167	102	13	150	0.13	1.52	0.58	4.01	$1.2 \cdot 10^4$	0.85	7.1	B
	208	180.7	123.5	31	160	0.31	1.64	0.52	4.7	$1.4 \cdot 10^4$	0.83	7.2	C
	238.6	224.8	155.4	24	160	0.24	1.85	0.62	6.1	$1.4 \cdot 10^4$	0.81	7.3	D

8.2 EXPLOSIVE LOADING

The experiments on spall strength measurements in non-stationary SW with the records of time function of stress $\sigma(t)$ at the interface "studied sample-PMMA" are shown in fig.18. The studied sample (3) in the disc form 10mm thick and 50mm in diameter which was pressed in the aluminium cartridge, was loaded in the contact explosion of plastic HE charge (2) of $\sigma_{HE}=10, 15$ and 20mm thickness which has density $\rho_{HE}=1.51\text{g/cm}^3$ and detonation velocity $D_{HE}=7.8\text{km/s}$ [10]. HE was initiated by the impact of 0.4-0.5mm thick aluminium foil of the plane detonation wave generator (1). The foil velocity at the moment of the impact against HE was $\sim 2.8\text{km/s}$. In this case the difference in time for the detonation wave front over the surface limited by 57mm diameter, did not exceed 0.13ms (see fig.19).

The stress profile $\sigma(t)$ at the sample-PMMA interface (5) was measured by a wire manganine gauge, the stress was calculated with the formula [1]:

$$\sigma = [34.5\Delta R/R + 7.5(\Delta R/R)^2], \text{ Gpa}$$

In ref.[1] the calculation technique for σ_p in σ - U_p coordinates according to the experimental values of σ_1 and σ_2 stresses is presented [11]. For the graphs, the shock adiabats were used in the form of linear U_s - U_p relationship for the studied sample:

$$U_s = 5.54 + 1.356 U_p, \text{ km/s} (\rho_0 = 2.77\text{g/cm}^3) \text{ (current work)}$$

and PMMA [12]:

$$U_s = 2.59 + 1.51 U_p, \text{ km/s} (\rho_0 = 1.18\text{g/cm}^3)$$

Table 9 sums up the experimental results, where σ_0 -maximal calculated stress in the sample at the interface with explosion products which was defined according to ref.[13]; σ_1^* -SW amplitude in the sample at 10mm depth (measured in individual tests when PMMA was substituted for 10mm thick sample).

Figure 20 presents $\sigma(t)$ oscillogram of SW in the sample at 10mm depth at $\delta_{HE}=10\text{mm}$. Figure 21 gives $\sigma(t)$ oscillogram at the sample PMMA interface at $\delta_{HE}=10\text{mm}$, characteristic points σ_1 and σ_2 are noted which were needed for σ_p calculation.

The comparison of table 8 and 9 results testifies for the fact that the increased intensity of the sample loading by more than an order does not result in the increased stress of aluminium composite stress ($\sigma_p=0.52$ - 0.65GPa at low intensity loading with the plate impact and $\sigma_p=0.57$ - 0.80GPa under explosive

loading), and the spall strength of the aluminium composite can be characterised by $\sigma_p = 0.62 \text{ GPa}$.

Table 9.

Results of Spall Strength Study under Explosive loading

HE charge thickness mm	Sample thickness mm	Stress GPa				σ_p
		σ_0^*	σ_1^*	σ_1	σ_2	
10	10	29.5	16.8	7.11	3.22	0.66
15	10	29.5	21.0	9.00	3.82	0.57
20	10	29.5		9.72	3.83	0.80

8.3 TEMPERATURE EFFECT

The study of the temperature effect on the aluminium composite spallation was conducted with calculation-experimental method [1] and microstructure analysis. The sample was loaded by the aluminium plate impact (110x150x4mm) accelerated by plastic HE explosion products ($\rho_0 = 1.51 \text{ g/cm}^3$, $D_{HE} = 7.8$ [10]). The impactor velocity was varied by changing the HE layer thickness. The tests were done both with and without sample heating to $+560^\circ$ temperature. Table 11 show the results of the study.

8.4 METALLOGRAPHIC STUDY

The degree and character of spallation as well as probable structural changes in the aluminium composite were studied with 3 types of thermally treated samples (see fig.22a,b,c). After shock-wave loading with heating and without heating. According to the observed destruction pattern, the degree of the material spallation is arbitrary divided in 4 stages:

D - complete spallation - separation of the whole spall layer;

B - intense microdestruction - substantial destruction available in the zone of spallation in the form of isolated or clustered cracks or pores;

C - slight microdestruction - small amount of isolated cracks or pores available in the spallation zone;

D - actually, no spallation.

Tables 10-11 give the data on the degree of spallation destruction of the studied samples, and figs. 23-26 show the character of their spallation.

As it is evident from the obtained results, the sample spall (fig. 22a, b) without heating is formed in the clustering of individual wide cracks or voids (figs.23b, 24b). The spall zone in the samples 5mm thick is formed at $\sim 3\text{mm}$ from the loaded surface, and in 10mm thick samples - at $\sim 7\text{mm}$ from the loading surface. The spall in the conical samples (fig.22c) without heating is also formed as a result of individual wide cracks or voids clustering (fig.25g), the spall zone is formed at $\sim 7\text{-}8\text{mm}$ from the loaded surface (fig.25b, c); with the increased load

to $W_0 = 460 \text{ m/s}$, except the partial spallation destruction the spall crossing the whole sample in thickness (fig. 25c) is also formed. In the conical samples with 560°C heating the spall is formed as a result of uniting of several individual pores (fig. 26g) and is a zone $\sim 3 \text{ mm}$ wide at $\sim 2 \text{ mm}$ from the loaded surface (fig. 26b).

Table 10

Results of Metallographic Study of
Sample Destruction

N sample types	W_0 m/s	Degree of spallation destruction
1a	112.0	actually no spallation destruction
2a	145.5	- " -
3a	156.7	- " -
4a	163.2	- " -
5a	173.9	- " -
6a	193.2	- " -
7a	208	intense microdestruction
8b	114.8	actually no spallation destruction
9b	123.1	- " -
10b	172.9	slight microdestruction
11b	166.9	- " -

Table 11

Results of Metallographic Study of
Sample Destruction in Temperature Effect Research

N sample type	$t^\circ \text{C}$	W_0 m/s	Degree of spallation destruction
1c	without heating	190	actually no spallation destruction
2c	- " -	240	slight microdestruction
3c	- " -	460	partial spallation destruction and complete destruction in the form of a spall
4c	560	100	actually no spallation destruction
5c	560	120	slight microdestruction

CONCLUSIONS

In the course of stage 3.2 of task 003 of subcontract 0002 P 0004-95 between RFNC - VNIIEF and LANL (USA) on the study of aluminium composite under VNIIEF dynamic loads:

- test samples of 10 dimension types were fabricated;
- composite micro- and macrostructure, microhardness were studied; non-uniform SiC particle distribution in the aluminium basis was revealed;
- elastic velocities ($C_L=7.16\text{km/s}$, $C_T=3.77\text{km/s}$), elastic moduli ($E=102.6\text{GPa}$, $K=89.2\text{GPa}$, $G=39.2\text{GPa}$, $\nu=0.308$) were identified;
- tension diagrams were determined at $T=25^\circ\text{C}$ and strain rates $\dot{\epsilon}=(200-260)\text{s}^{-1}$ as well as the compression diagrams at $T=-50, 25, 100, 300^\circ\text{C}$ and relative $\dot{\epsilon}=(200-500)\text{s}^{-1}$;
- crack resistance was identified at $T=-50, 25, 100, 300^\circ\text{C}$; at relative impact velocities $(0.63-1.4)\cdot 10^4\text{s}^{-1}$, a wear crack resistance of the composite is noted;
- dynamic deformation at $\dot{\epsilon}\approx 10^3-10^4\text{s}^{-1}$ is described by the elastic-plastic model of constant ultimate yield $\sigma_r=0.4\text{GPa}$;
- dynamic ultimate yield function was studied as a difference in the main stresses under shock wave compression. In 2.3-2.2GPa stress range the ultimate dynamic yield Y_g is almost constant and constitutes 0.24GPa;
- it was found that the magnitude of the spallation strength for the aluminium composite is almost constant $\sigma_p=0.62\text{GPa}$ in 1-2GPa to 29GPa stress range;
- detailed metallographic study was accomplished to learn the degree of spallation destruction character in the loaded samples.

REFERENCES

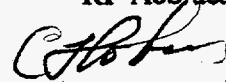
1. Report on contract 0002 P 0004-95 (Task 003). Study of destruction and resistance to plastic deformation for aluminium composite under dynamic loads. Methods. Novikov S.A., Bat'kov Yu.V., Polyakov L.V. et al. VNIIEF, 1995.
2. D.S.Hughes, W.I.Pondrom and R.L.Mims. Transmission of Elastic Pulses in Metal Rods. Phys., v.75, N10, 1949.
3. RD 50-344-82. Methodological instructions Identification of crack resistance characteristics under dynamic loading. M. Izd-vo standartov, 1983.
4. L.V.Al'tshuler. Shock wave application in high pressure physics. UFN, 85(2), 1965, p. 197.
5. L.V.Al'tshuler, A.A.Bakanova, I.P.Dugoladov, E.A.Dynin, R.F.Trunin, B.S.Chekin. Shock adiabats of metals. New data, statistical analysis and universal laws. PMTF, N2, 1981, p.3.
6. Properties of condensed substances under high pressures and temperatures. Collection of articles edited by R.F.Trunin. Minatom, CNII upravleniya, ekonomiki i informatzii, 1992.
7. Jones S., Gills P., Foster J. On the equation of motion of the underformed section of a Taylor impact // J. Appl. Phys. - 1987-61. N2-p.499-502.
8. Novikov S.A., Petrov V.A.. Explosive facilities for mechanical tests of materials and constructions (Review). M. CNIIAtominform, 1983, p.37.
9. V.N.Mineev, V.P.Pogorelov, A.G.Ivanov et al. Facilities for composite material and construction behaviour study under dynamic loading. FGV, 1978, N3.
10. S.A.Novikov. Strength under quasistatic and shock wave loading. FGV, 1985, N6, p.77-85.
11. Yu.V.Bat'kov, A.B.Glushak, S.A.Novikov. Manganine gange applications for spallation phenomena study in metals under explosive loading. In book: All-Union meeting on detonation. Presentations. 1988, v.1, p.154-157.
12. Yu.V.Bat'kov, V.K.Golubev, S.A.Novikov et al. On spallation destruction recording in copper and lead under explosive loading. FGV., 1988, N1, p.89-92.
13. S.A.Kinelovskii, Yu.A.Trishin. On the decomposition calculation at interface HE-condensed matter. FGV, 1984, N1, p.126-133.

RFNC - VNIIEF
LosAlamos National Laboratory

Material Behaviour Study under Quasistatic Loading
(3 stage of task 003 of contract 0002P0004-95)

Contract manager

RF AoS academician



Novikov S. A

Principal Investigator

Polyakov L. V.

Abstract

According to the requirement of 3.4 stage of task 003 subcontract 0002P0004-95 between RNFC-VNIIEF and LANL (LosAlamos National Laboratory), the research of aluminium composite of 20% weight SiC was conducted under quasistatic loading ($\dot{\epsilon} = (10^{-4} - 10^{-3}) \text{ s}^{-1}$)

In (-70-300) °C temperature range the values of mechanical properties σ_b , $\sigma_{0.2}$, δ and ψ were identified as well as elastic characteristics E and ν ; strain diagrams $\sigma - \epsilon$ were built.

The experiments done to obtain $\sigma(\epsilon)$ functions at temperatures (400-500) °C with σ and δ characteristic identification.

Contents

Introduction	4
1.Experiment arrangement	5
2.Research results	6
3.Conclusion	7
4.References	8

Introduction

The study of mechanical properties of the aluminium composite at different temperatures (from -70°C to $+300^{\circ}\text{C}$) under quasistatic (10^{-4} - 10^{-3}) s^{-1} loading is the stage of works for contract 0002P0004-95. The previous report [1] gives the techniques for material experimental research.

1. Experiment arrangement

The aluminium composite properties were studied with samples after thermal treatment :

- 1) regime T6 : exposure - 8 hours at $T = 530^{\circ}\text{C}$ with water cooling at $T = 65-70^{\circ}\text{C}$.
- 2) aging at $T = 154^{\circ}\text{C}$ for 5 hours with air cooling.

The samples were cut out of the blank across (1) and along (2) the axis.

The test samples are presented in fig. 1.

Type 1 samples were used to identify the elastic characteristics of the material, E and ν . The longitudinal and transversal strains were measured with tensoresistors KF5P1 and digital tensometric bridge CTM-3 at 10 o.e.g. measurement accuracy. The tensoresistors were glued on the sample in longitudinal (2 pieces) and transversal (1 piece) direction

Characteristics E and ν were identified to $T = 200^{\circ}\text{C}$ (the operation limit for the tensoresistors).

Type 2 samples were used to define mechanical characteristics σ_b , $\sigma_{0,2}$, δ and ψ and to obtain $\sigma - \epsilon$ diagrams. To record " force-absolute extension " diagram, the sample strain was measured with 2 Smm base extensor. The tests were accomplished at traverse velocity of $V=1,67*10$ m/s. The properties were studied in -70°C to 300°C temperature range

Type 3 sample were used in the experiments on material behaviour at 400°C and 500°C temperatures. With them characteristics σ_b and δ were identified as well as function $\sigma (\epsilon)$. At 500°C the test were done with three impact velocities.

In total 16 samples of type 1, 25 samples of type 2 and 8 samples type 3 were tested. The samples were exposed at specified temperature for 30-60 min (depending on the temperature). The exposure time was defined with a control sample in the middle of which a thermopair was mounted.

The test were located at INSTRON 1185 facility.

2. Research Results.

Table 1 and figure 2 (averaged results for 2-3 samples) give the material mechanical characteristic dependent on temperature for two direction of sample cuttings. The statistics analysis of the obtained results was not accomplished because the amount of the tested samples is too small. Figure 3a gives typical functions $\sigma(\epsilon)$ at different temperatures.

Tension diagrams for 20 , 100 and 200 °C temperatures were built with " force - sample extension " diagram data. For -70 °C and +300 °C temperatures they were obtained via recalculations of computer diagrams " force - traverse motion " with the technique isted in ref. [2].

Mechanical characteristics.

Table 1.

* - characteristics for the given temperature are presented according to sample 1. Table 2 presents the experiment results (by samples) at 400 °C and 500 °C temperatures. Figure 3.b gives $\sigma(\epsilon)$ functions at 400 °C (sample 2) and 500 °C (samplse 3).

Strength and Plasticity at high Temperatures.

Table 2.

Analysing the experiment results we must mention their instability which is especially evident at high temperatures This is seen by the table 2 results for 500 °C temperature.

Probably, this fact can be explained by insufficiently homogenous material structure with non-unifom distrifution of carbide phase that was revealed in metallographic reseach.

Table 1

Mechanical characteristics

sample cutting direction	T	σ_b	$\sigma_{0.2}$	δ	ψ	E	ν
	°C	MPa		%		GPa	
I	-70	-	-	-	-	103.9	0.305
	-50	-	-	-	-	103.8	0.293
	24	305	270	0.7	2.2	102.6	0.298
	100	290	250	-	-	100.3	0.280
	150	270	240	1.0	2.6	-	-
	*200	255	240	1.2	2.5	95.0	0.305
	*290	70	65	7.0	14	-	-
II	-70	335	330	0.24	1.3	104.0	0.270
	-50	330	320	0.26	1.0	103.2	0.305
	24	320	300	0.5	1.0	102.3	0.313
	100	309	280	0.7	1.5	100.9	0.318
	200	260	245	0.9	2.0	91.9	0.306
	290	72	68	5.0	16.5	-	-

* - characteristics for the given temperature are presented according to sample 1.

Table 2.

Strength and Plasticity at high Temperatures

T	$\dot{\epsilon}$	N	σ_b	δ
°C	c ⁻¹		MPa	%
400	0.7*10 ⁻³	1	41	8.5
		2	38	9.2
500	0.35*10 ⁻³	1	19	10.
		2	12	20.
	0.7*10 ⁻³	3	12	30.
		4	20	26.
	1.4*10 ⁻³	5	14	30.
		6	22	20.

3. Conclusion

We can note the following based on the aluminium composite study :

- sample cutting direction does not substantially affect material properties;
- elastic modulus magnitude increases negligibly with temperature increase to 200 °C. Poisson's coefficient is practically always constant and constitutes 0.30 ;
- with temperature increase from -70 °C to +200 °C a certain decrease in strength (10-20 %) and insignificant increase in plasticity are seen, the material is deformed uniformly; at 300 °C an abrupt decrease in strength and plasticity growth occur deformation becomes localized ; this process continues at 400 °C and 500 °C also, finally ultimate strength value drops from 320 MPa at room temperature to 16 MPa at 500 °C, the extension grows from 0.5% to 28%, respectively ;
- at 500 °C $\dot{\epsilon}$ rate variation in (0.35 - 1.4) * 10⁻³ s⁻¹ range does not affect the composite properties.

4. Referens

1. Novikov S. A., Bat'kov Yu. V., Glushak B. L.

Study of destruction and resistance to plastic deformation of aluminium composite under dynamic loading. Methods.

(1 stage of 003 task of contract 0002P0004-94). Arzamas-16, 1995.

2. Korshunov A.I., Kravchenko T.N., Saveleva O.M.\,

Plotting stress-strain diagrams by recalculation of the computer diagram Strength Mater.-1982-v14, N9 p.1268-1271.

Test samples

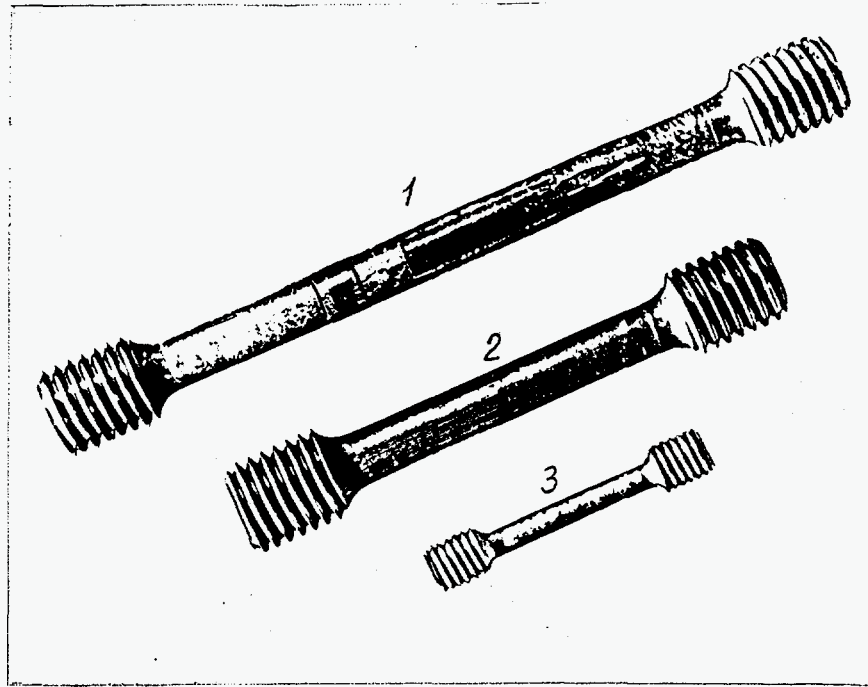


Fig.1

Dependence of mechanical characteristics of aluminium composite on temperature and sample cut direction.

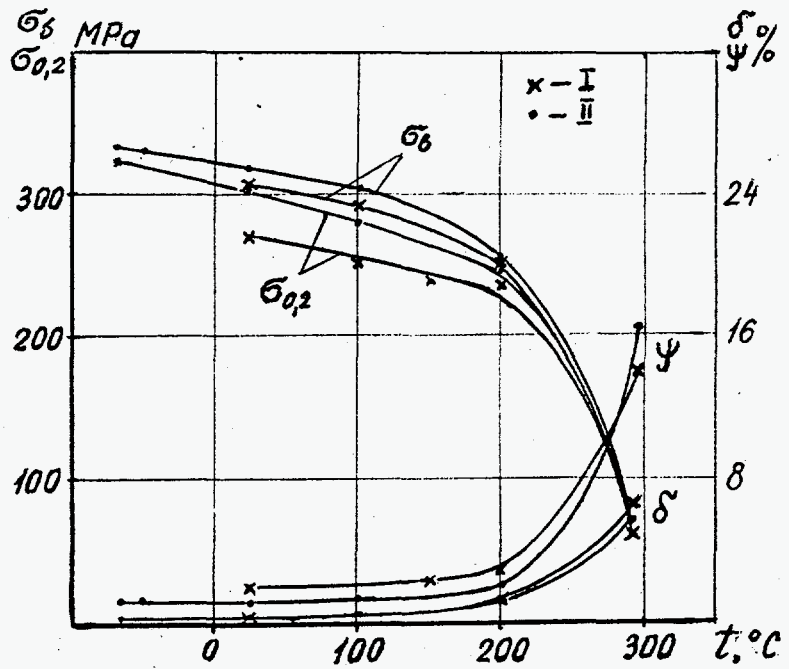


Fig.2

Aluminium composite extension diagrams of different temperatures.

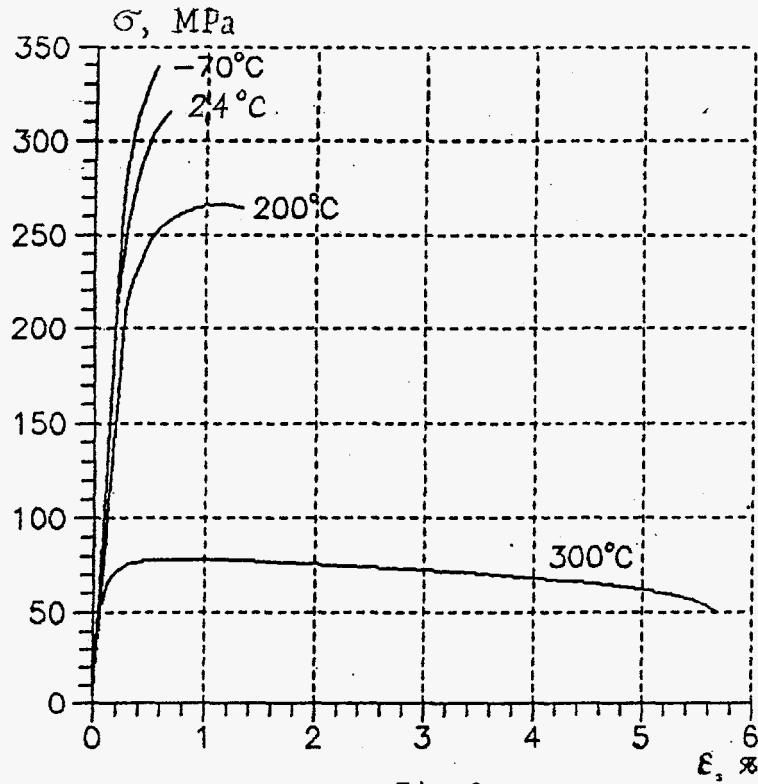


Fig.3.a

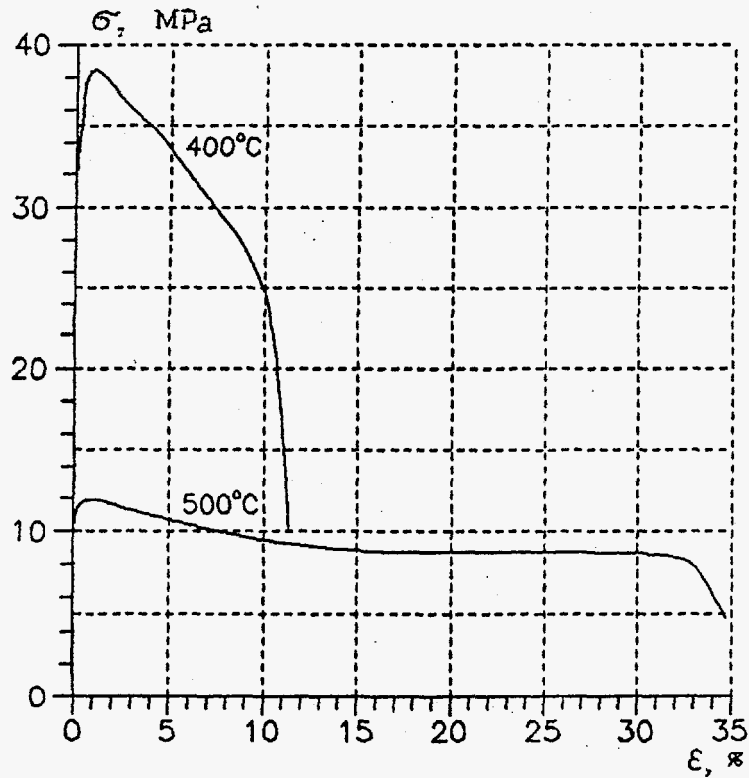


Fig.3.b

Blank Cutting Geometry for Sample Fabrication

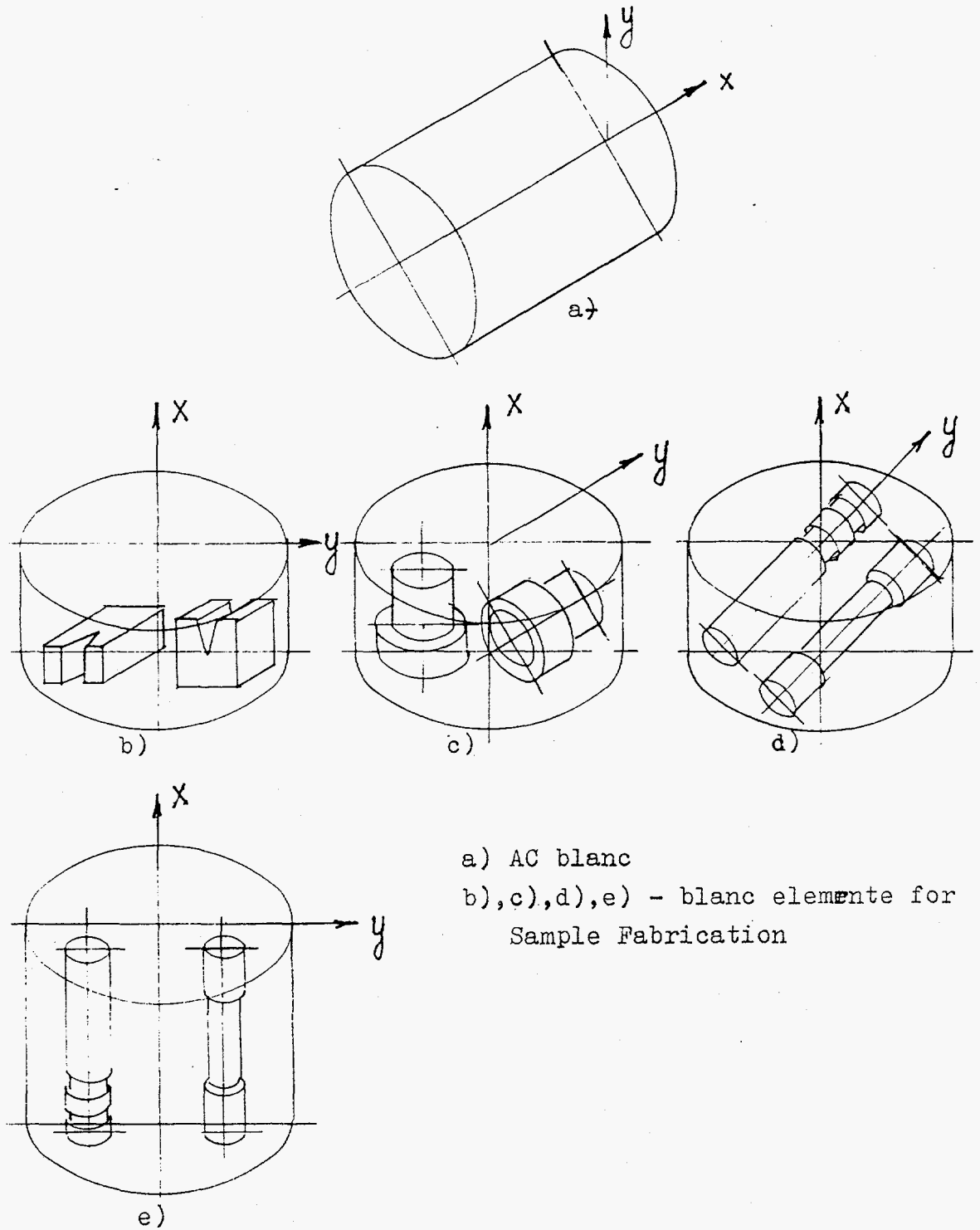
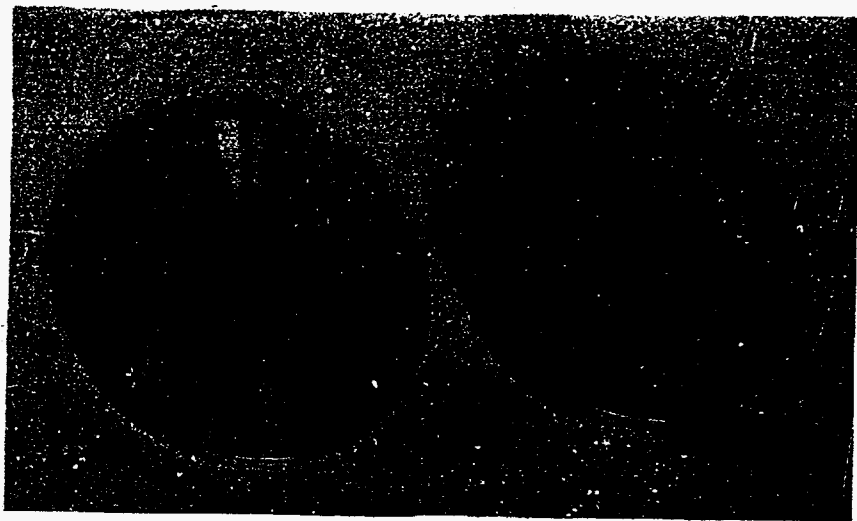
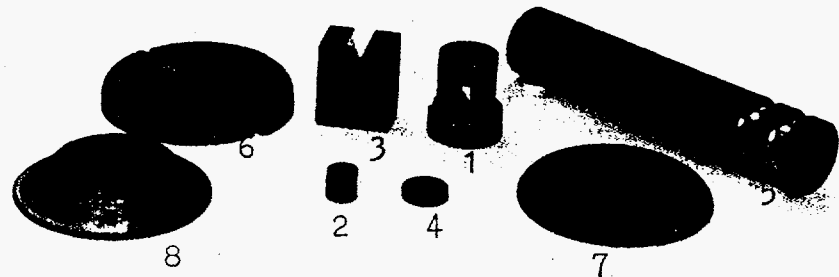


Fig. 1

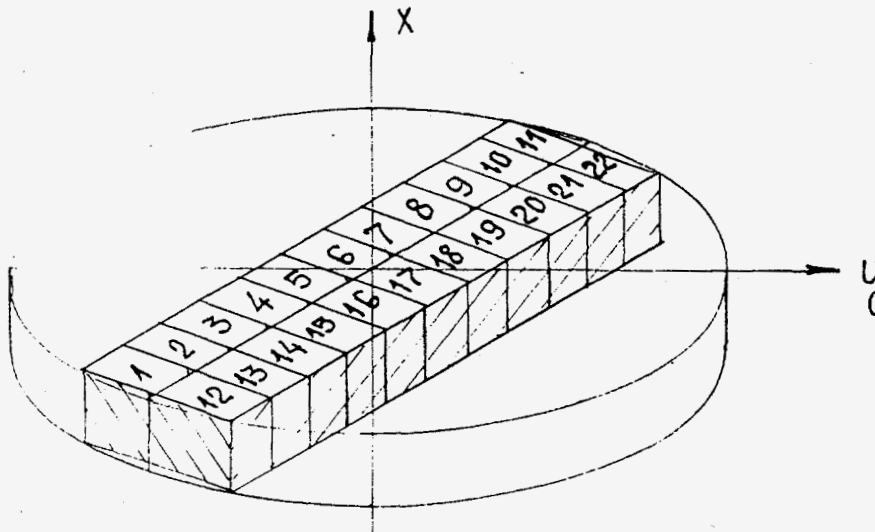
sample photographs for dynamic
property study



- | | | |
|---------------------|--------|-------|
| 1 -tension | 6 - } | shear |
| 2 -compression | 7 - } | |
| 3 -crack resistance | 8 - } | spall |
| 4 -compressibility | 9 - } | |
| 5 -ultimate yield | 10 - } | |

Fig. 2

Cutting of Wigners-Sampler for
Metallographical Study

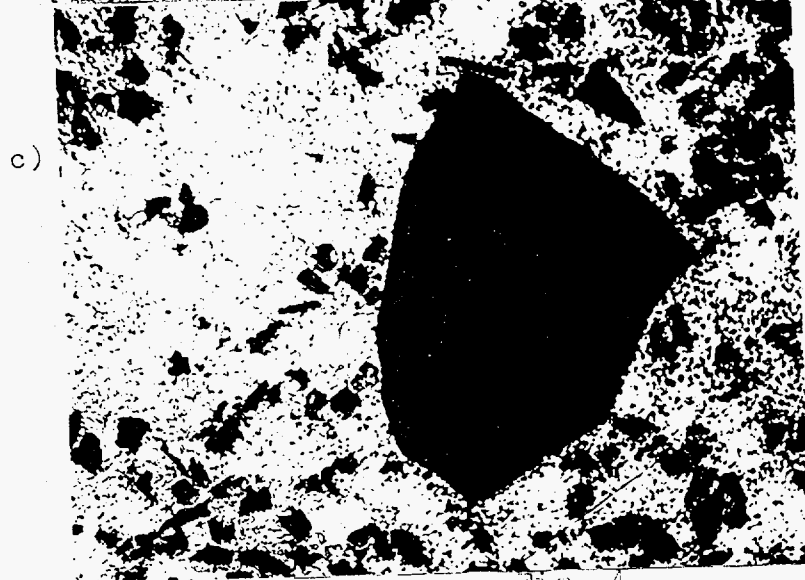
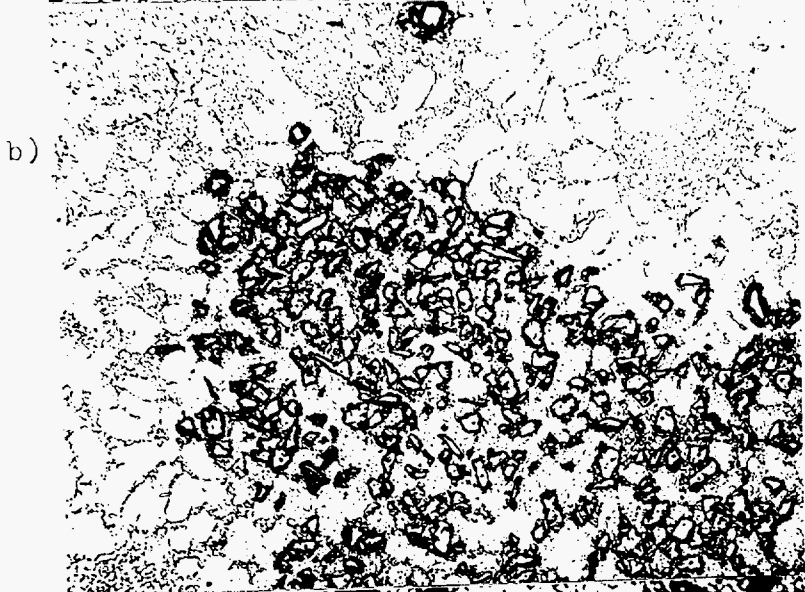


Sample surfaces microsection
fabrication

Sampler NN 1 - 11 - as received

Sampler NN 12 - 22 - after thermal treatment

Fig.3



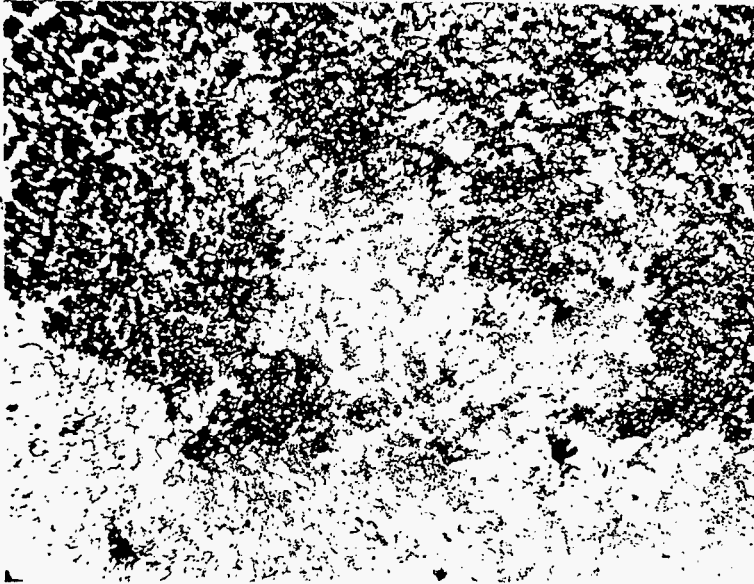
Solid solution of aluminium with silicon

Eutectics of aluminium with silicon

Particks in aluminium basis

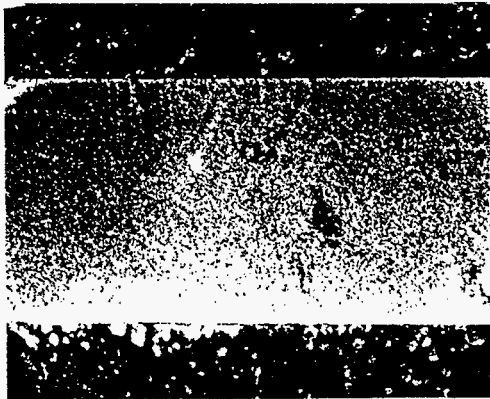
Large partick

Aluminum
basis with
SiC



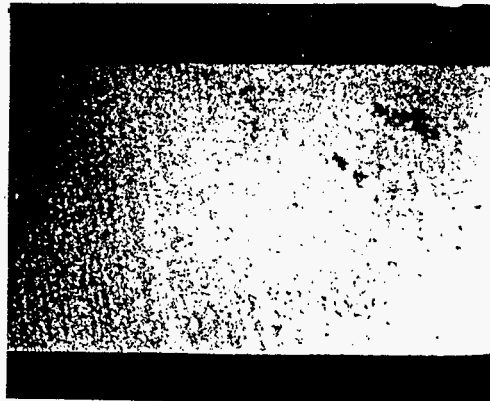
(c)

Aluminum basis
without SiC



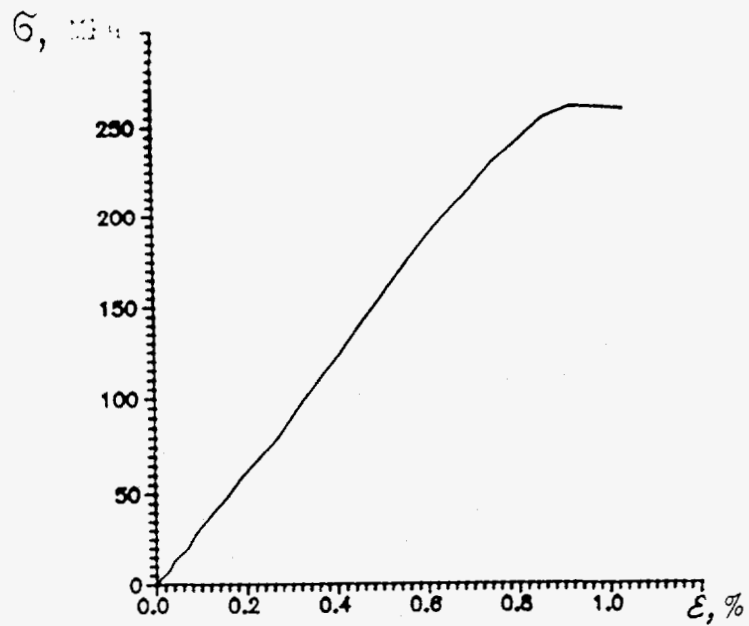
(b)

Aluminum basis
without SiC

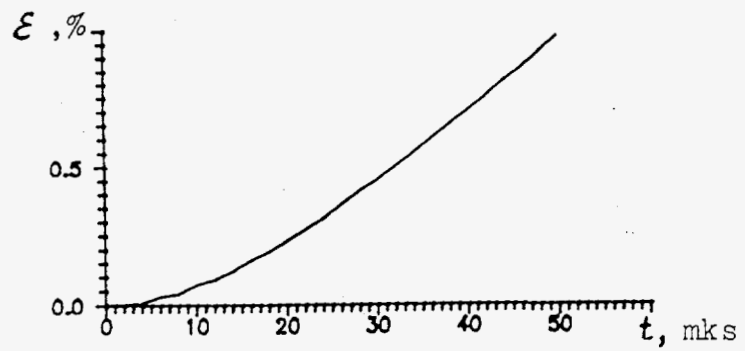


(a)

Test 1, dynamic tension, $\dot{\epsilon} = 200 \text{ s}^{-1}$, $T = 25 \text{ }^\circ\text{C}$



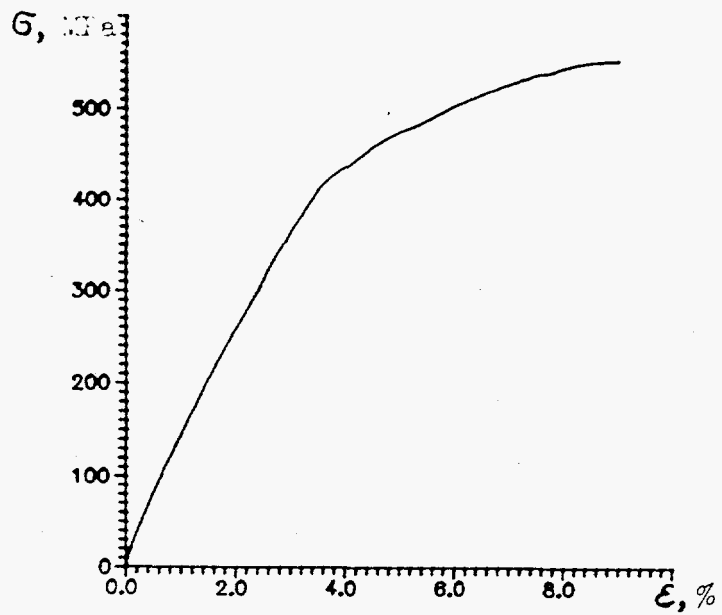
a) diagram of stress-strain $\sigma-\epsilon$



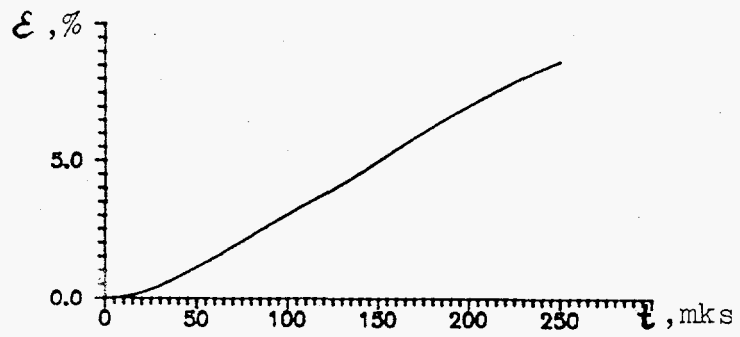
b) strain-time curve $\epsilon = \epsilon(t)$

Fig. 6

Part 4, dynamic compression, $\dot{\epsilon} = 390 \text{ s}^{-1}$, $T = 25 \text{ }^\circ\text{C}$



a) diagram of stress-strain $G-\epsilon$



b) strain-time curve $\epsilon = \epsilon(t)$

Fig. 7

Test 5. crack resistance, $\bar{V}=1,40 \cdot 10^4 \text{ s}^{-1}$, $T=25 \text{ }^\circ\text{C}$

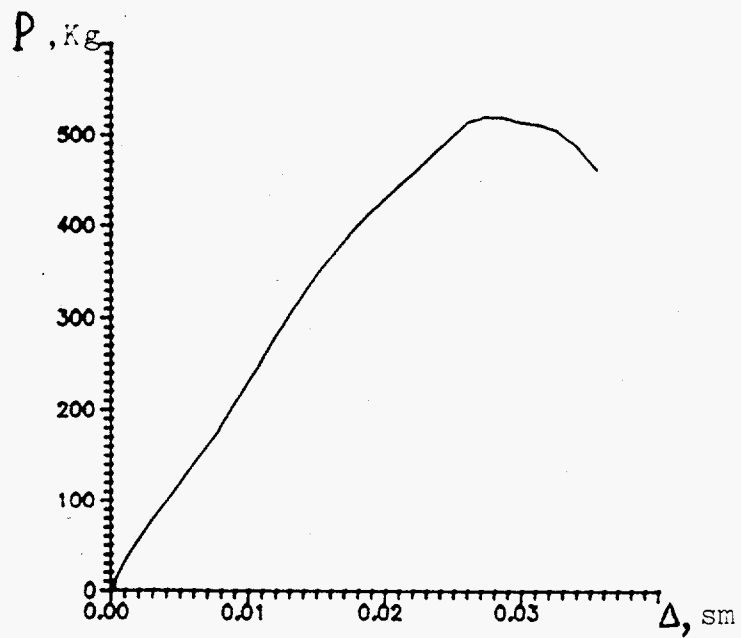


Fig. 3.

U_s - U_p - Diagram for Aluminium Composite

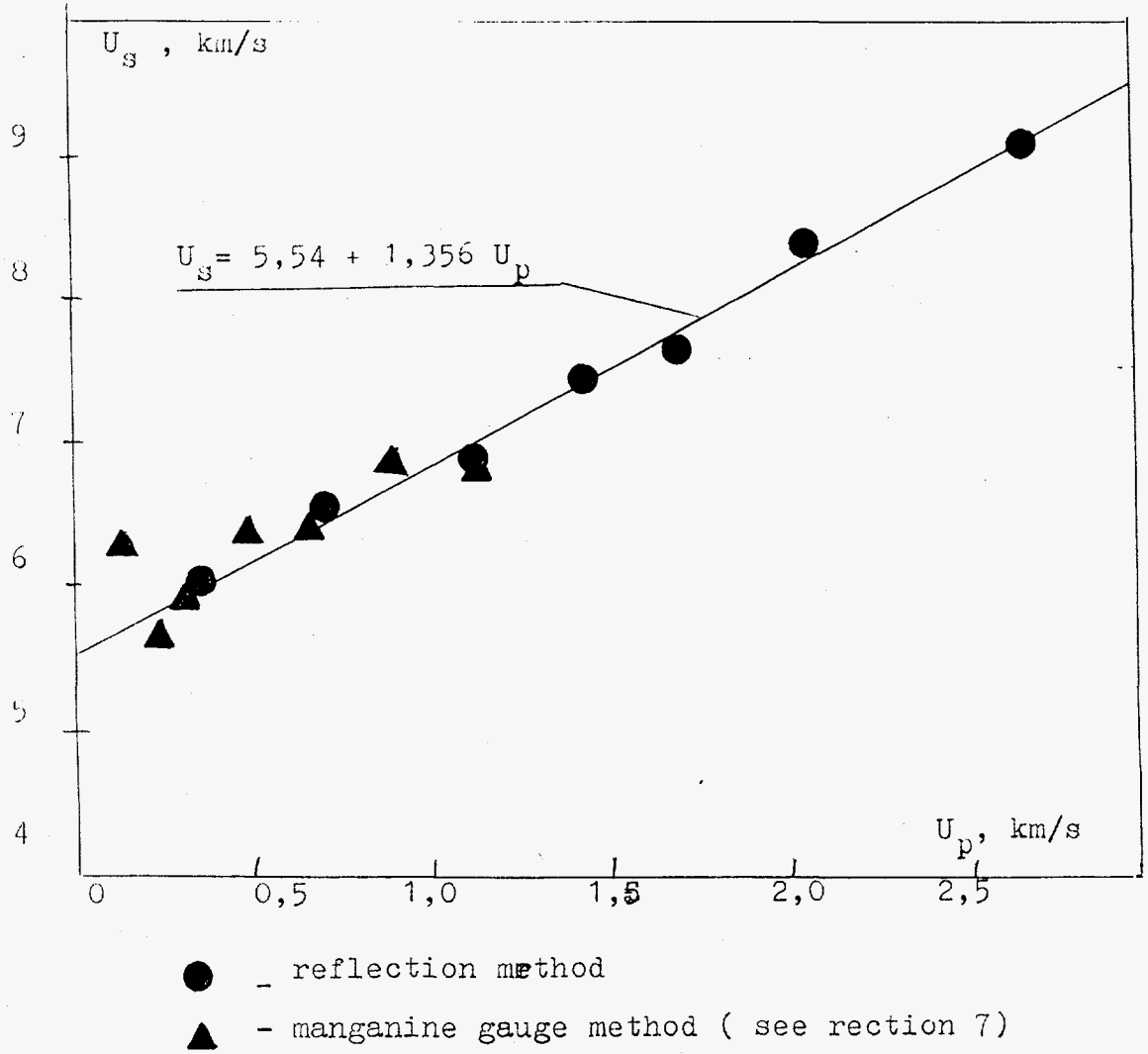


Fig. 9

Aluminium Composite Samples before before and
after Impact

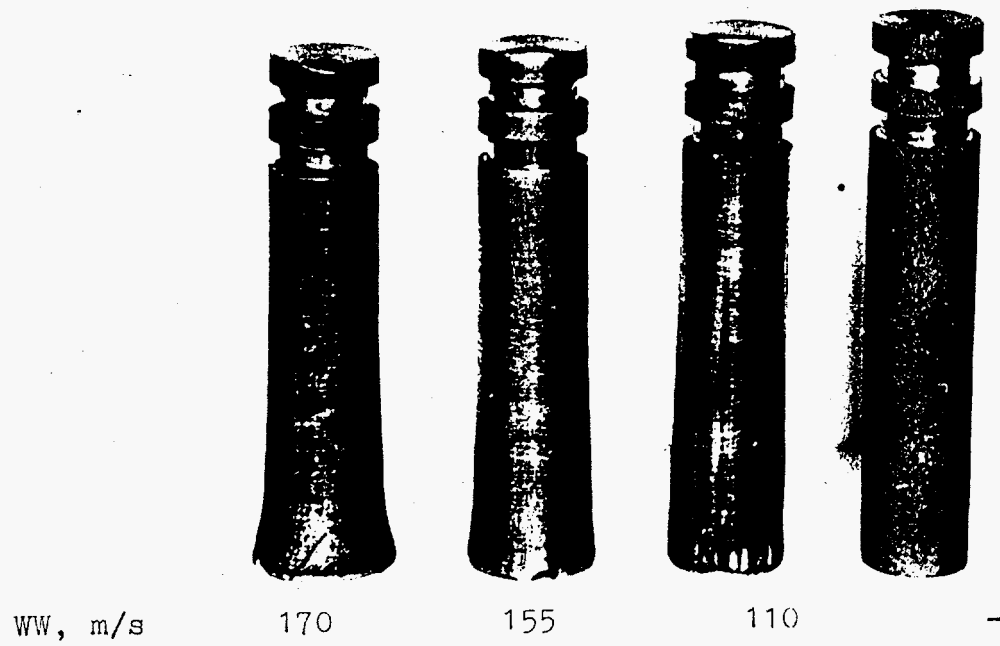


Fig. 10
Calculation Results

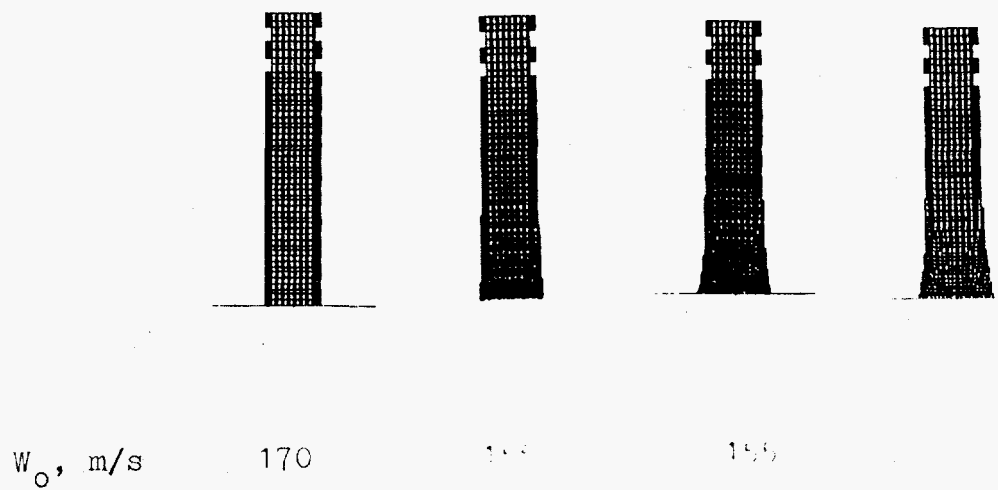
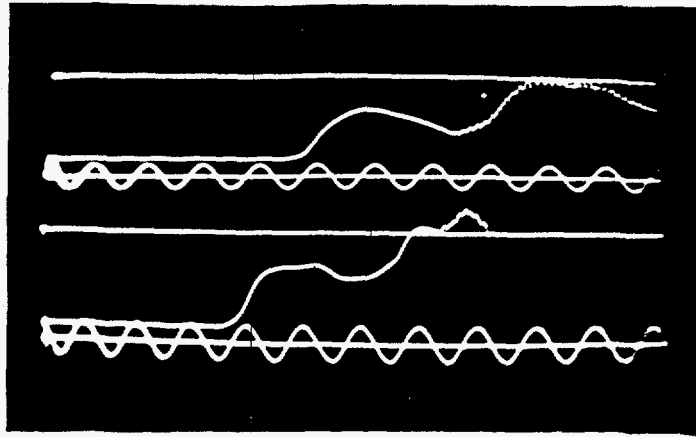


Fig. 11

Main Stress Oscillidgrams

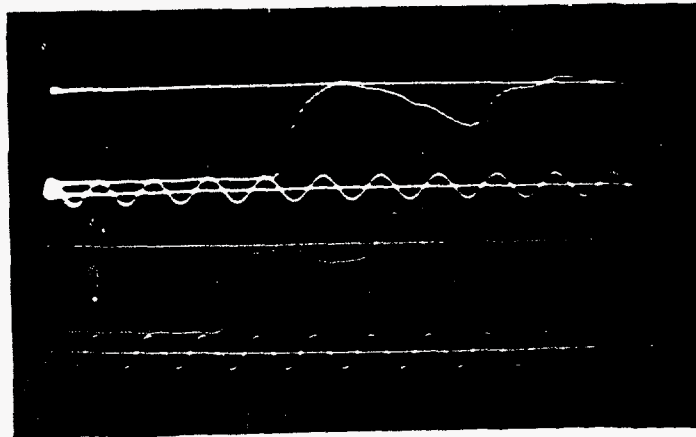
a)



$$\sigma_y = 2,0 \text{ GPa}$$

$$\sigma_x = 2,4 \text{ GPa}$$

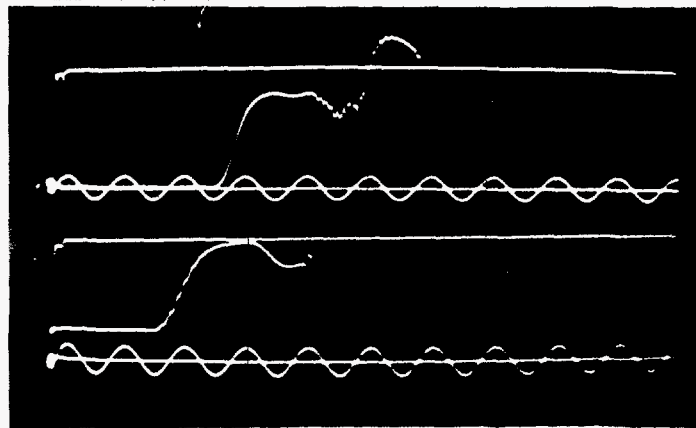
b)



$$\sigma_y = 3,3 \text{ GPa}$$

$$\sigma_x = 3,6 \text{ GPa}$$

c)

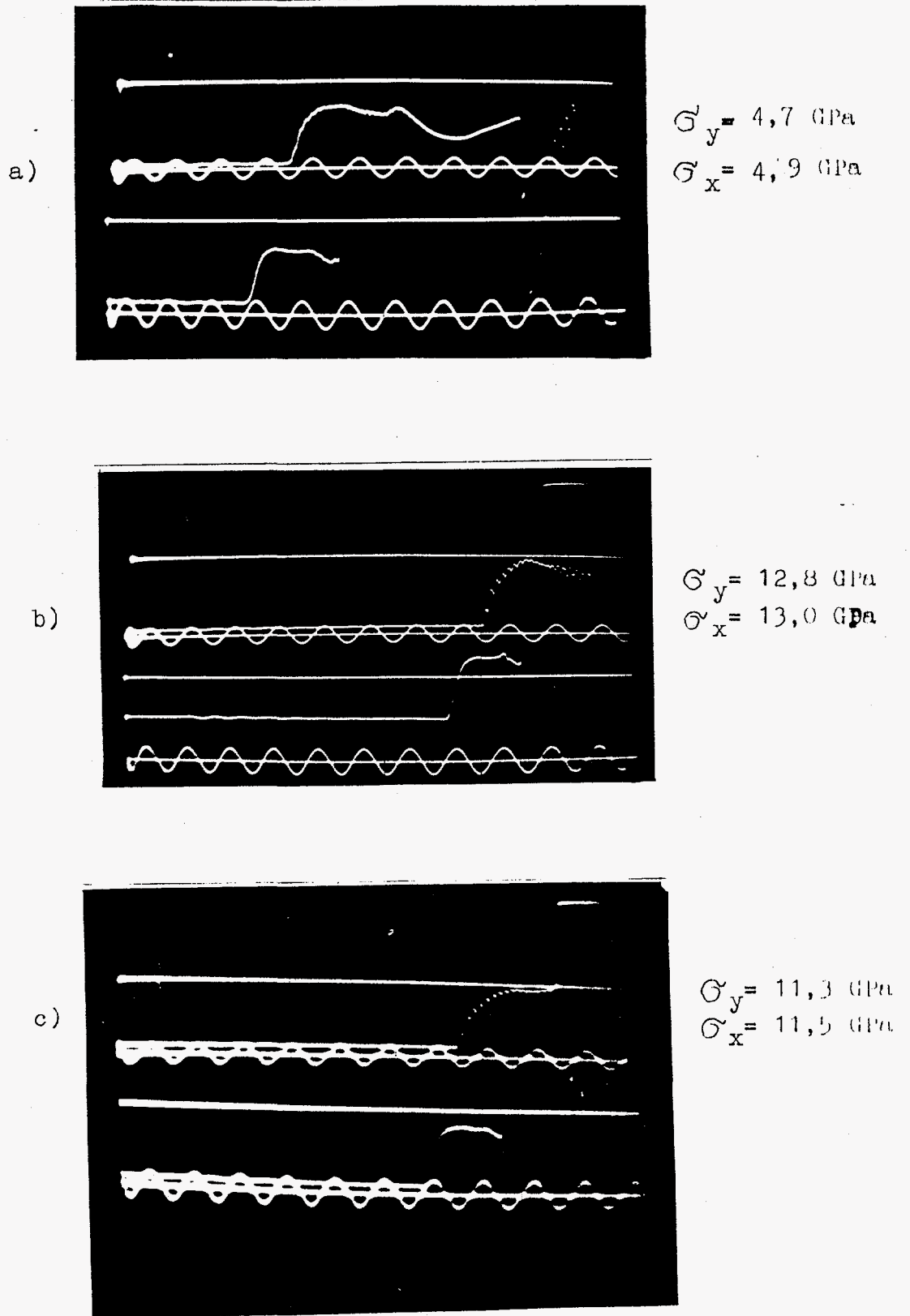


$$\sigma_y = 3,6 \text{ GPa}$$

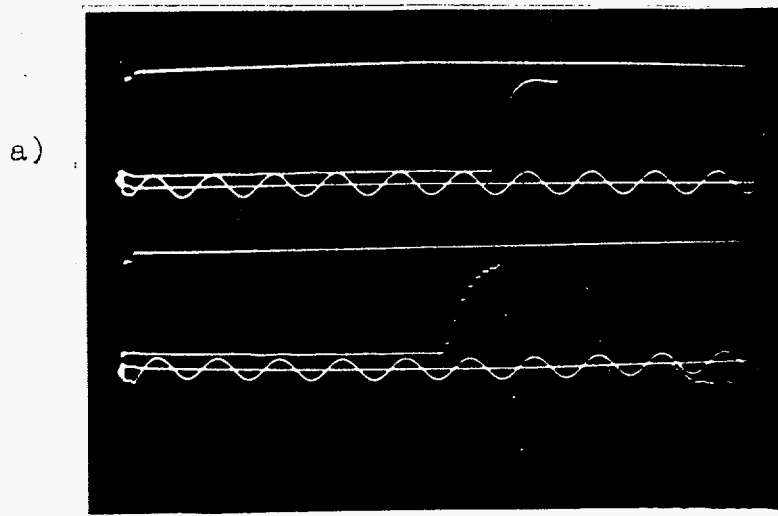
$$\sigma_x = 3,8 \text{ GPa}$$

Time interval - 1 μs

Main Stress Oscillograms

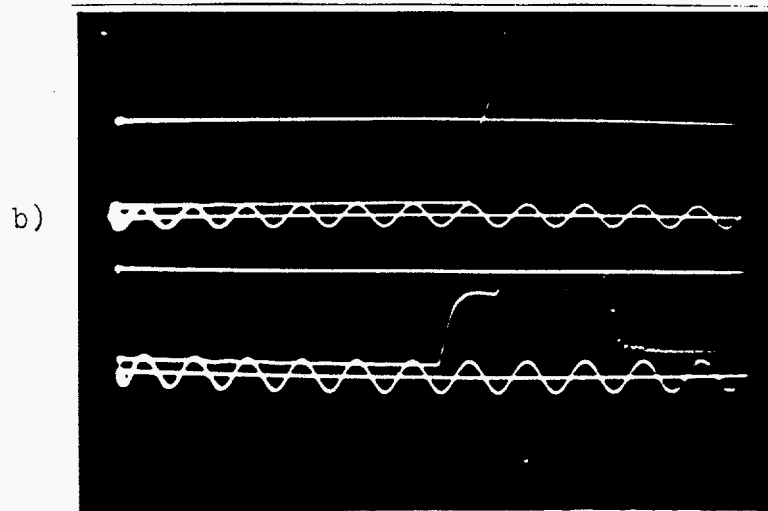
Time interval - 1 μ s

Main Stress Oscillograms



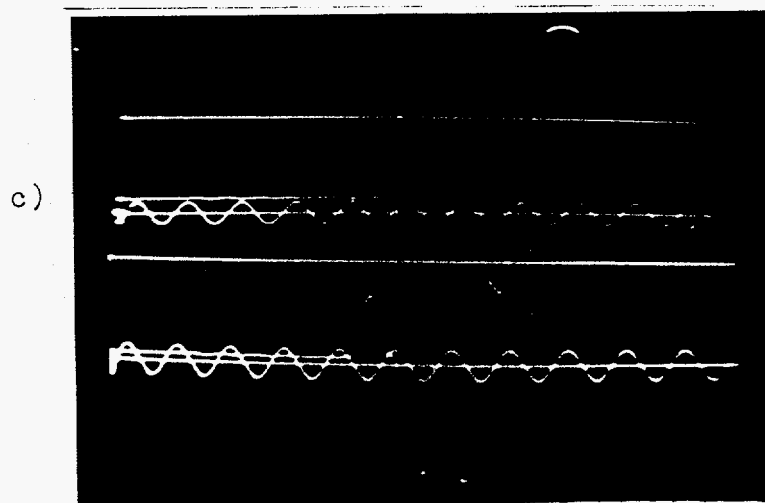
$$\sigma_{x_2} = 16,9 \text{ GPa}$$

$$\sigma_{x_1} = 16,8 \text{ GPa}$$



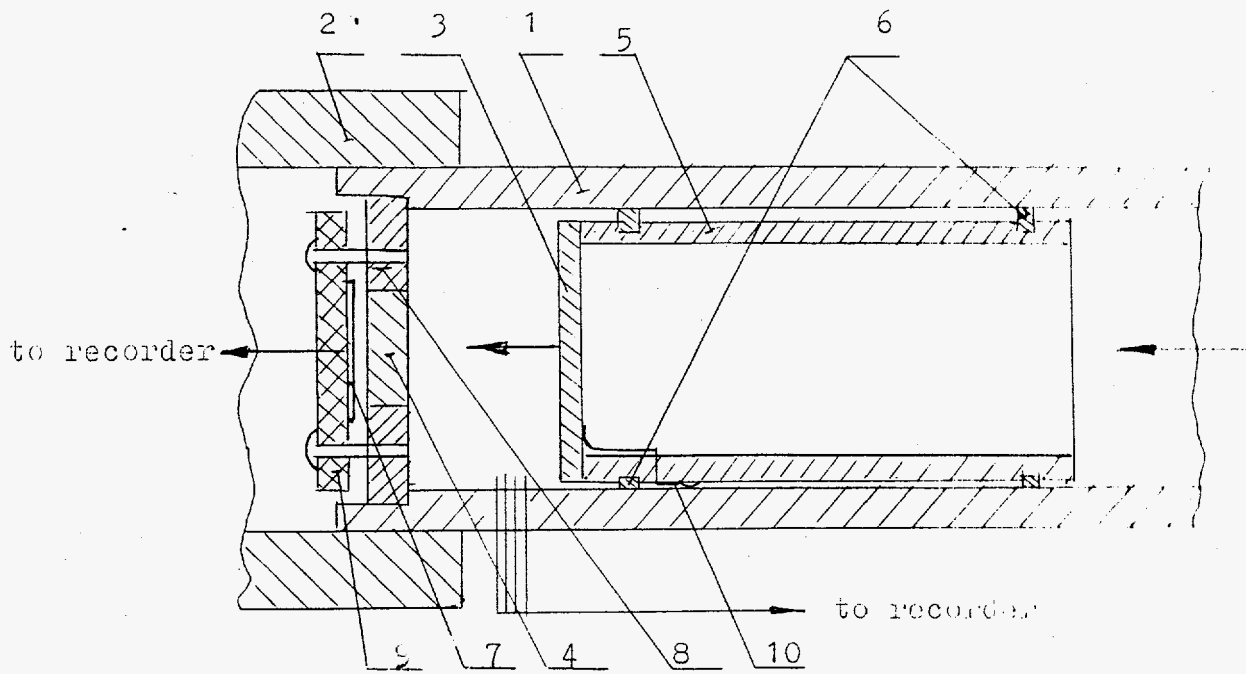
$$\sigma_y = 16,6 \text{ GPa}$$

$$\sigma_{x_2} = 16,9 \text{ GPa}$$



$$\sigma_y = 21,6 \text{ GPa}$$

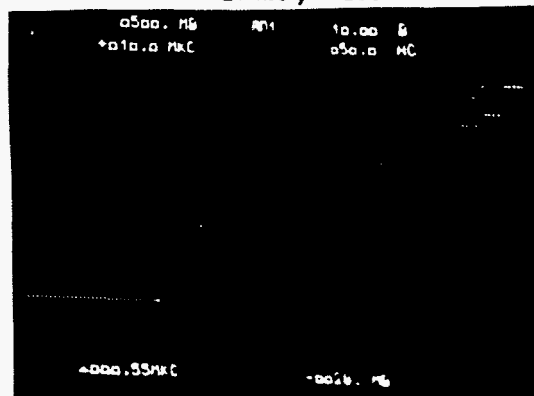
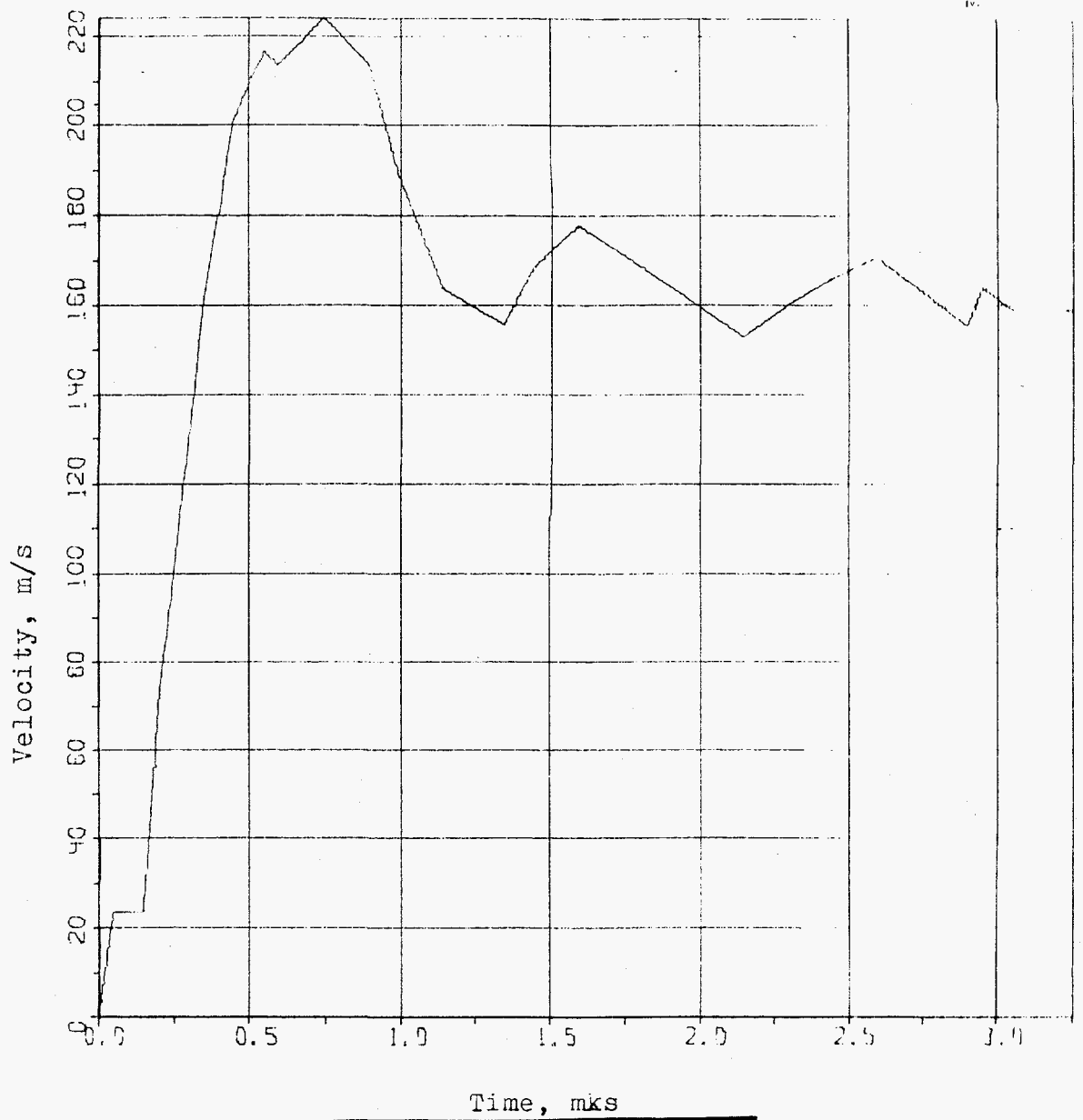
$$\sigma_x = 21,3 \text{ GPa}$$



1. Barrel headpiece
2. Braking chamber
3. Impaktor
4. Sample
5. Shell
6. Fluoroplastik rings
7. Capacitive gauge
8. Sample cartridge
9. Isolator
10. Impaktor kontakt with facility casing

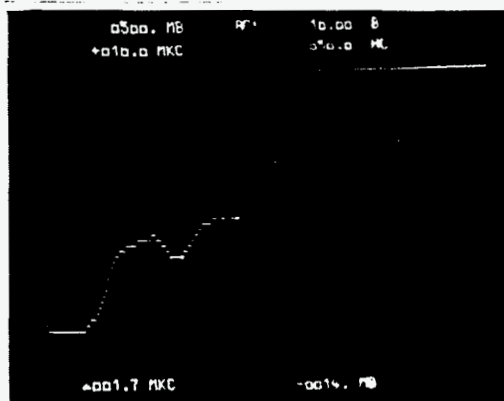
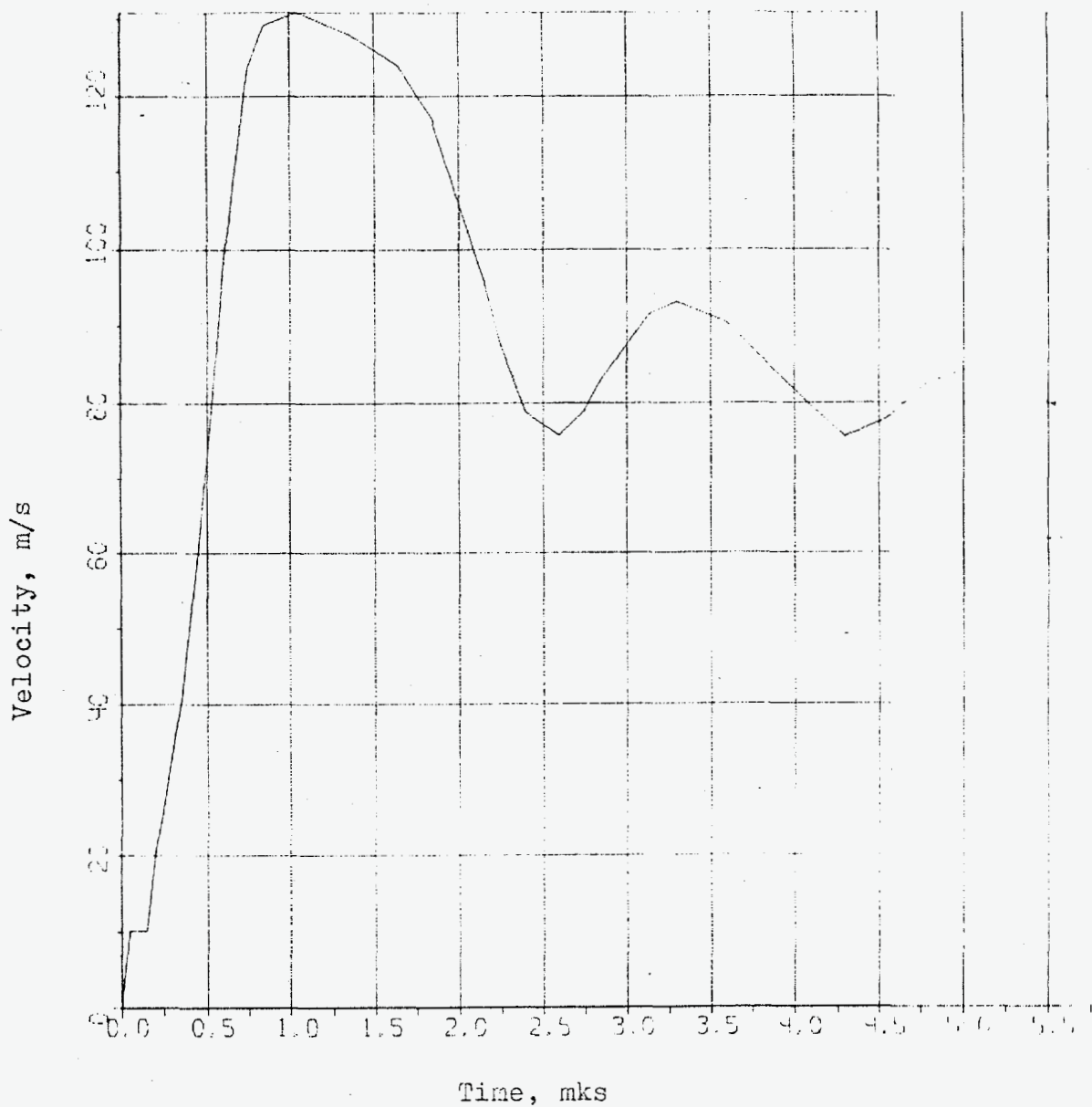
Fig. 15

Free surface velocity $\Delta_m = 5 \text{ mm}$



Capacitive gauge $\delta(t)$ oscillogram

Free surface velocity $\Delta_m = 10 \text{ mm}$



Capacitive gauge output oscillogram

Fig. 17

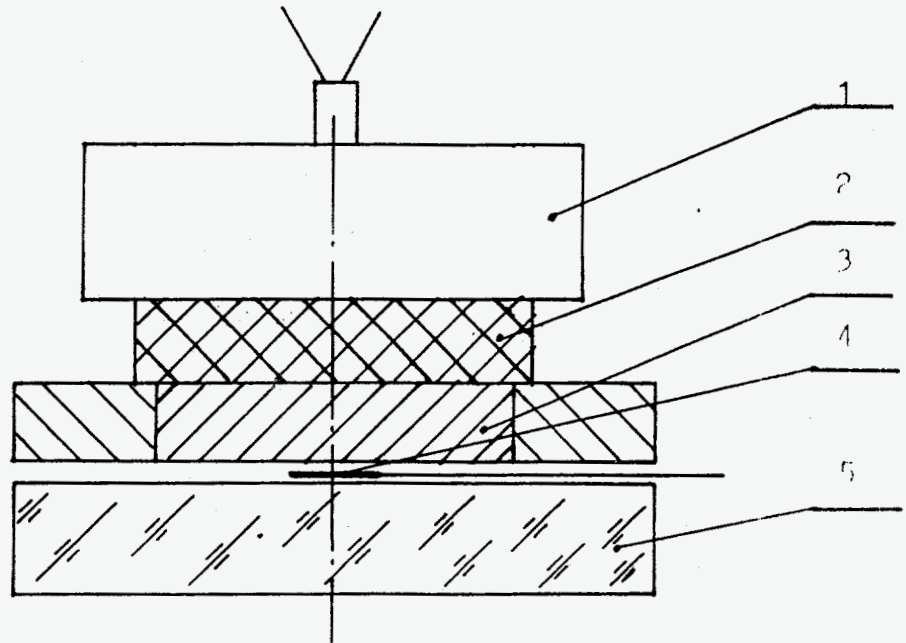
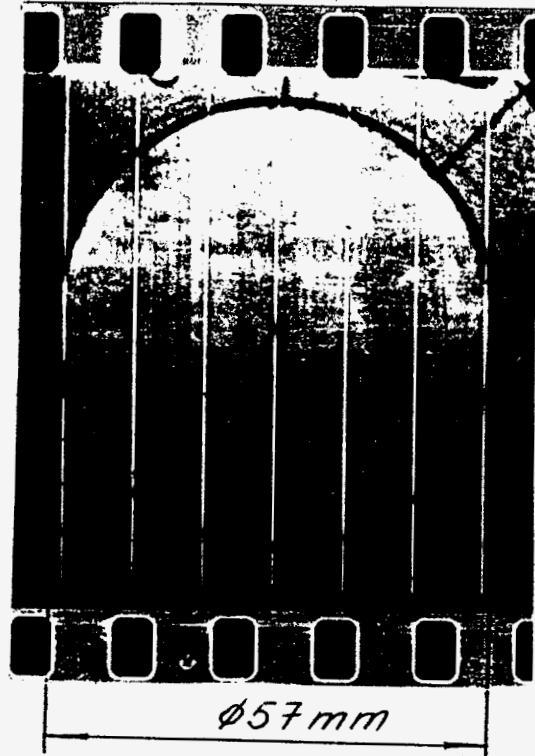


Fig.18. Experimental setup

preliminary frame



frame under the process

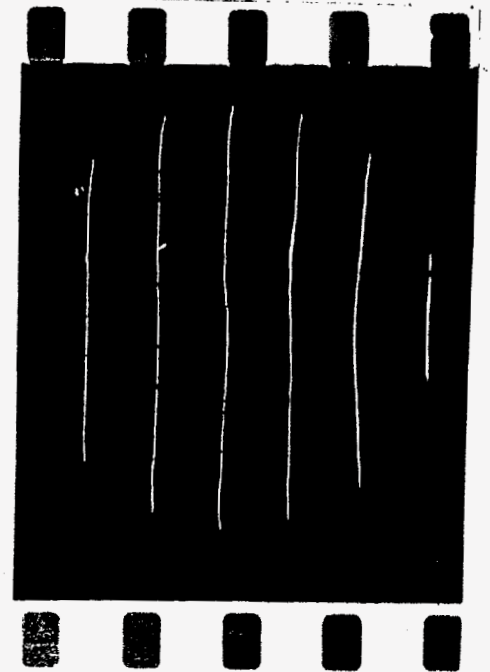
 $V = 3 \text{ mm}/\mu\text{s}$

Fig.19. Detonation wave front photochronogram

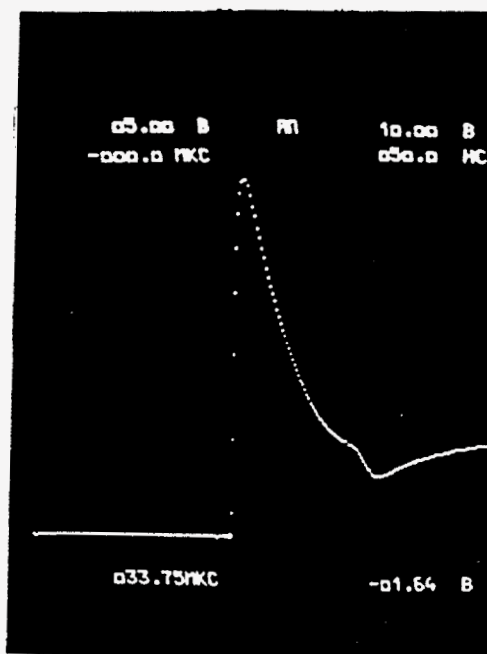


Fig.20. Oscillogram $\sigma(t)$ of the passing shock wave.

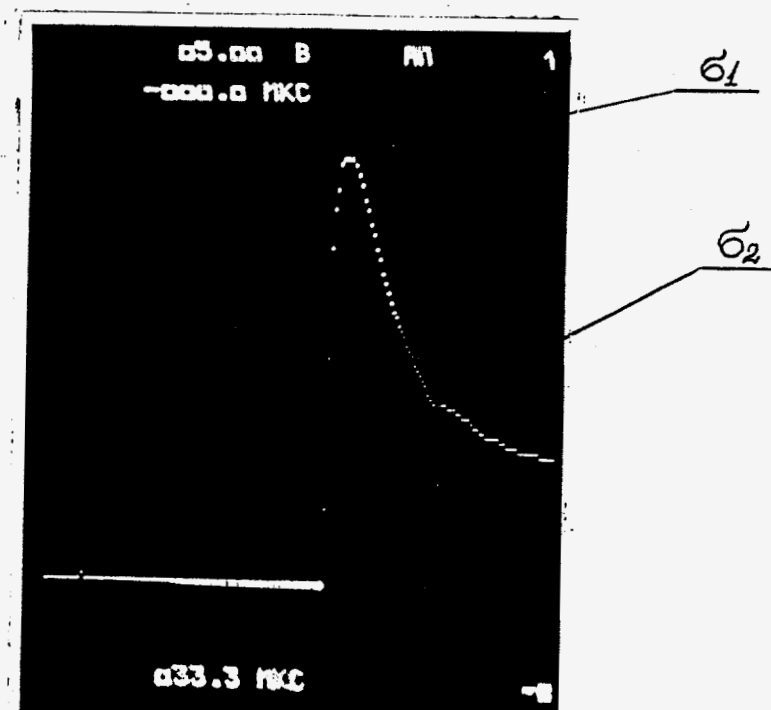
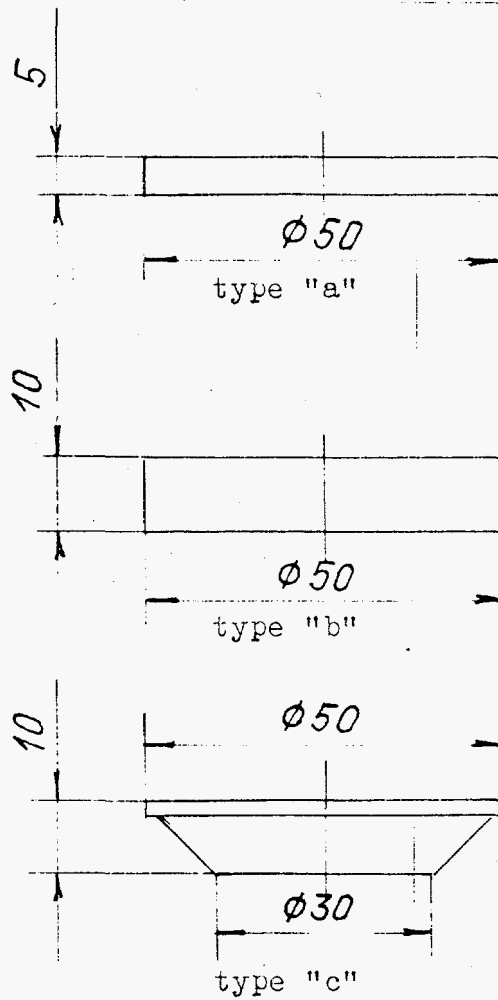


Fig.21. Oscillogram $\sigma(t)$ of the specimen-PMMA boundary.

Sample types for metallographic
after shock waves impact



loaded surface - upwards

Fig. 22

Spallation character of type "a" samples
without heating

a)



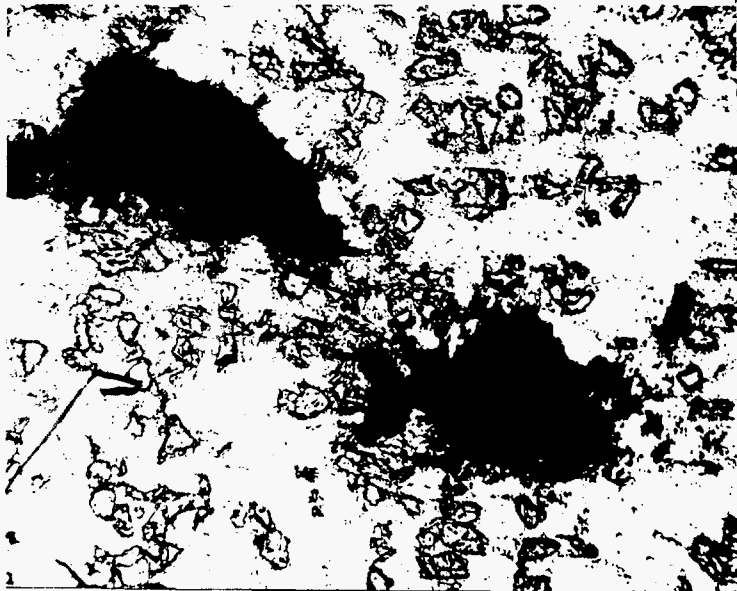
x 5 - no spallation

b)



x 5 - intense microdestruction

c)

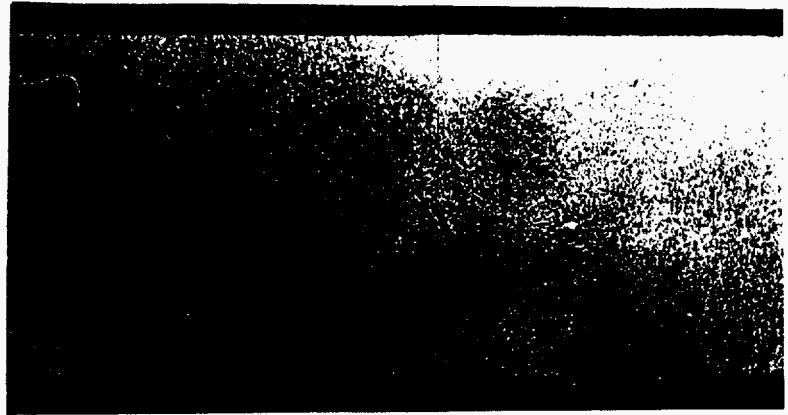


x 200 - spallation character

Fig.23

Aluminium Composite Microstructure

a)



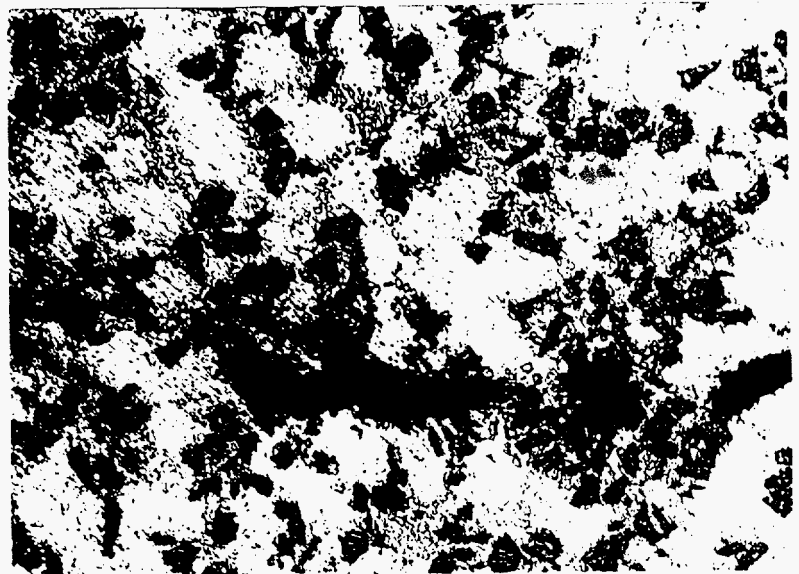
Aluminium
basis with

b)



Aluminium
basis
without

c)

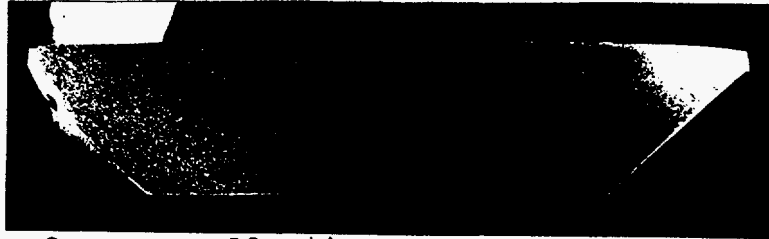


Aluminium
basis
without

Fig. 24

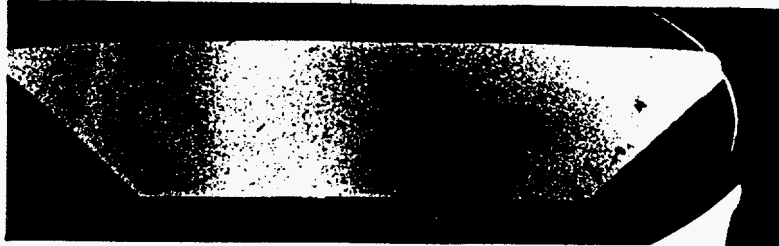
Spallation destruction character of type "c" samples
without heating

a)



x2 - no spallation

b)



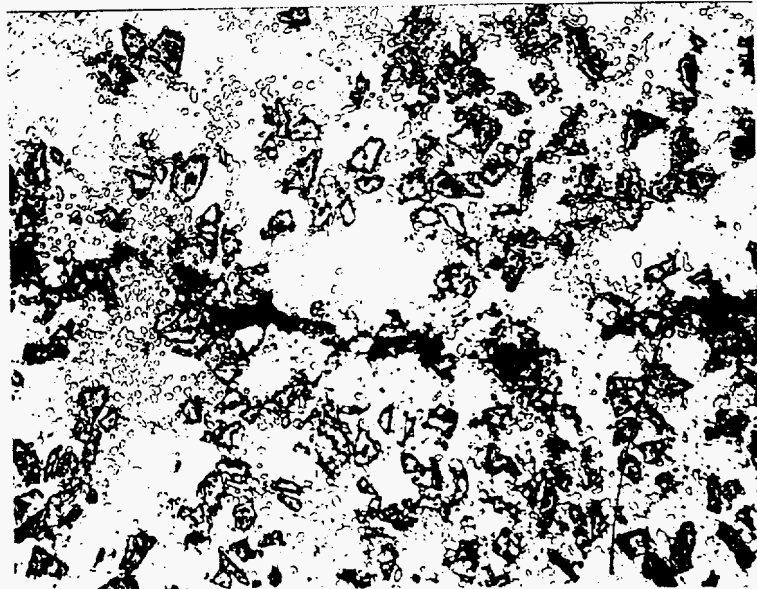
x2 - weak microdestruction

c)



x2 - partial spallation

d)



x 300 - spallation microdestruction character

Spallation destruction character of type "c" samples
at 300°C heating



x 2 - no spallation



x 2 - Weak microdestruction



x 300 - spallation microdestruction